Geochemistry Geophysics Geosystems G3
AN ELECTRONIC JOURNAL OF THE EARTH SCIENCES
Published by AGU and the Geochemical Society

Article
Volume 7, Number 3
3 March 2006
Q03002, doi:10.1029/2005GC001094
ISSN: 1525-2027

Temperature variations at diffuse and focused flow hydrothermal vent sites along the northern East Pacific Rise

Daniel S. Scheirer
Department of Geological Sciences, Brown University, Providence, Rhode Island 02912, USA

Now at U.S. Geological Survey, MS 989, 345 Middlefield Road, Menlo Park, California 94025, USA (dscheirer@usgs.gov)

Timothy M. Shank
Department of Biology, Woods Hole Oceanographic Institution, Woods Hole, Massachusetts 02543, USA

Daniel J. Fornari
Department of Geology and Geophysics, Woods Hole Oceanographic Institution, Woods Hole, Massachusetts 02543, USA

[1] In the decade following documented volcanic activity on the East Pacific Rise near 9°50′N, we monitored hydrothermal vent fluid temperature variations in conjunction with approximately yearly vent fluid sampling to better understand the processes and physical conditions that govern the evolution of seafloor hydrothermal systems. The temperature of both diffuse flow (low-temperature) and focused flow (high-temperature) vent fluids decreased significantly within several years of eruptions in 1991 and 1992. After mid-1994, focused flow vents generally exhibited periods of relatively stable, slowly varying temperatures, with occasional high- and low-temperature excursions lasting days to weeks. One such positive temperature excursion was associated with a crustal cracking event. Another with both positive and negative excursions demonstrated a subsurface connection between adjacent focused flow and diffuse flow vents. Diffuse flow vents exhibit much greater temperature variability than adjacent higher-temperature vents. On timescales of a week or less, temperatures at a given position within a diffuse flow field often varied by 5°–10°C, synchronous with near-bottom currents dominated by tidal and inertial forcing. On timescales of a week and longer, diffuse flow temperatures varied slowly and incoherently among different vent fields. At diffuse flow vent sites, the conceptual model of a thermal boundary layer immediately above the seafloor explains many of the temporal and spatial temperature variations observed within a single vent field. The thermal boundary layer is a lens of warm water injected from beneath the seafloor that is mixed and distended by lateral near-bottom currents. The volume of the boundary layer is delineated by the position of mature communities of sessile (e.g., tubeworms) and relatively slow-moving organisms (e.g., mussels). Vertical flow rates of hydrothermal fluids exiting the seafloor at diffuse vents are less than lateral flow rates of near-bottom currents (5–10 cm/s). The presence of a subsurface, shallow reservoir of warm hydrothermal fluids can explain differing temperature behaviors of adjacent diffuse flow and focused flow vents at 9°50′N. Different average temperatures and daily temperature ranges are explained by variable amounts of mixing of hydrothermal fluids with ambient seawater through subsurface conduits that have varying lateral permeability.

Components: 12,006 words, 13 figures.

Keywords: hydrothermal systems; East Pacific Rise; vent fluids; seafloor eruptions.

Index Terms: 3017 Marine Geology and Geophysics: Hydrothermal systems (0450, 1034, 3616, 4832, 8135, 8424); 3035 Marine Geology and Geophysics: Midocean ridge processes; 9355 Geographic Location: Pacific Ocean.

Received 31 July 2005; **Revised** 11 October 2005; **Accepted** 19 December 2005; **Published** 3 March 2006.

Scheirer, D. S., T. M. Shank, and D. J. Fornari (2006), Temperature variations at diffuse and focused flow hydrothermal vent sites along the northern East Pacific Rise, *Geochem. Geophys. Geosyst.*, *7*, Q03002, doi:10.1029/2005GC001094.

1. Introduction

[2] Mid-ocean ridge (MOR) hydrothermal vents represent the seafloor expression of a complex system of heat and mass transfer between newly formed, cooling oceanic crust and the ocean water column. Studies of hydrothermal fluid venting shed light on the mechanisms governing these transfers, and they are particularly illuminating in the aftermath of well-constrained crustal accretion events such as dike emplacement, volcanic eruption, fissuring, or faulting. In addition to physical and chemical exchange, the evolution of hydrothermal systems is critical to the development and structure of associated biological communities.

[3] Typically, seafloor hydrothermal vents are classified into two distinct types: those characterized by vigorous, focused outflow at high temperatures and those characterized by diffuse low-temperature flow. Focused flow discharge is generally >100°C, often between 300°–400°C, and it creates polymetallic mounds and steep-sided chimneys that range in height from a few meters to several tens of meters. Diffuse flow venting typically takes place through low mounds and cracks that are often occupied by biological communities, and the venting fluids are usually <50°C. Estimates of the relative proportion of heat transferred by focused and diffuse flow vary among investigators, techniques, and study area. Diffuse flow represents 100% at sites where focused venting is absent (e.g., at fields along the Galápagos Spreading Center [*Corliss et al.*, 1979]), >80% on the Endeavor Segment of the Juan de Fuca (JdF) Ridge [*Schultz et al.*, 1992], and ~67% on the Cleft Segment of JdF Ridge [*Baker et al.*, 1993]. This proportion likely varies significantly with different phases of the crustal accretion process.

[4] Diffuse flow hydrothermal vents have received less study than their higher-temperature counterparts [*Von Damm and Lilley*, 2004]. Diffuse flow fluid temperature and composition differences from seawater are not as extreme as at focused flow vents, and they do not provide long-lived orifices to facilitate sampling of minimally-diluted fluids during repeat visits to individual vent sites. Nonetheless, the major proportion of biomass associated with seafloor hydrothermal systems resides within and adjacent to diffuse flow sites. Furthermore, developing faunal assemblages can modify the discharge environment in these settings [*Shank et al.*, 1998; *Sarrazin and Juniper*, 1999].

[5] The physical and chemical mechanisms governing MOR hydrothermal activity have been inferred primarily through observational and modeling studies. Surveying and sampling are typically conducted on single or repeat field programs to particular hydrothermal sites which, to date, have been concentrated in the east and northeast Pacific and the north Atlantic oceans. Physical models of hydrothermal systems have been developed and refined since the recognition several decades ago of the oceanic heat flow deficit near mid-ocean ridges [*Langseth and von Herzen*, 1970]. The important unknowns of these models are: the sites of recharge into the hydrothermal system, the subsurface pathways that fluids follow from recharge to discharge, the locations of fluid reaction, mixing, and storage, and the response of various components of the system to events such as igneous intrusion, volcanic eruption, and tectonic faulting and fissuring. Interactions between the hydrothermal fluids that discharge from the seafloor and the local hydrography, currents, and topography lead to a rich array of plumes, hydrothermal deposits and constructions, and biological communities. In the past 15 years, time series studies have provided an important perspective of hydrothermal systems that is complementary to that gained by discrete field visits. Monitoring the temperatures of individual vents is the easiest continuous observation to make in situ. Time series observations of chemical constituents and ocean currents at vents are becoming more common [e.g., *Luther et al.*, 2001; *Marsh et al.*, 2001]. The remote monitoring of MOR seismicity has been extremely helpful in identifying igneous and tectonic activity that may be associated with changes in hydrothermal activity [*Dziak et al.*, 1999; *Johnson et al.*, 2000; *Fox et al.*, 2001; *Smith et al.*, 2002].

[6] Previous time series temperature studies of MOR hydrothermal systems have ranged in du-

ration from hours to ~0.5 year [e.g., *Little et al.*, 1991; *Schultz et al.*, 1996; *Fujioka et al.*, 1997; *Fornari et al.*, 1998; *Tivey et al.*, 2002], although recent studies have increased deployment durations [*Dziak et al.*, 2003; *Reves-Sohn et al.*, 2005; this study]. These investigations generally observed insignificant or very slow temperature variations at focused flow vents, unless there was a discrete crustal accretion event. In contrast, diffuse flow temperatures vary significantly at periods of tens of minutes to weeks. Much of this variability occurs at semidiurnal (~12 hr) and diurnal (~24 hr) tidal periods and near periods of inertial motions and storm systems at the ocean surface.

[7] The aim of the present study is to demonstrate how variations in the temperature of diffuse flow hydrothermal vents, following a volcanic eruption near 9°50′N on the East Pacific Rise (EPR), can be used to elucidate (1) the origin of diffuse flow fluids, (2) their interactions with near-bottom currents, (3) their connections with adjacent focused flow venting, and (4) their influence and dependence on associated faunal communities. Discrete temperature measurements at many of the EPR vent sites were made soon after the eruption [*Haymon et al.*, 1993] and approximately once per year in the 11 years that followed [*Shank et al.*, 1997; *Von Damm*, 2000, 2004].

[8] Fundamentally, temperature is a quasi-conservative property in this setting, and temperature variations provide a basic and relatively easy-to-measure method of detecting changes in the hydrothermal circulation associated with each vent. Because heat flow drives the hydrothermal circulation, it is reasonable to expect that vent fluid temperatures reflect both the cooling of magmatic bodies at depth and the modification of permeability through progressive cracking or sealing. In addition, elevated temperatures facilitate rock-seawater interactions and biogeochemical reactions that lead to the deposition of metalliferous hydrothermal precipitates and to the development of biological communities rooted in chemosynthesis. Finally, the mixing of oxygenated seawater and reduced hydrothermal fluids provides an environment where redox pairs (such as sulfate-sulfide, carbon dioxide-methane, ferric-ferrous iron) can be exploited by vent-endemic and associated fauna. Temporal and spatial changes in this environment have shaped the evolution and biogeography of hydrothermal vent fauna worldwide [e.g., *Sarrazin and Juniper*, 1999; *Shank et al.*, 1998; *Copley et al.*, 1999].

2. Study Area

[9] The seafloor near 9°50′N on the EPR (Figure 1) has been extensively studied following a well-documented series of volcanic eruptions in early 1991 through early 1992; prior observations in this area provided a baseline for studying changes to the geologic, hydrothermal, and biological systems following these eruptions [e.g., *Haymon et al.*, 1991, 1993; *Rubin et al.*, 1994; *Lutz et al.*, 1994; *Von Damm*, 1995, 2000; *Shanks et al.*, 1995; *Shank et al.*, 1998; *Mullineaux et al.*, 1998; *Shanks*, 2001; *Von Damm and Lilley*, 2004]. The eruptions in the early 1990s produced lobate and sheet lavas that span ~9 km along the spreading axis (Figure 1b). Lava lakes filled the 5–10 m deep axial summit trough (AST), and subsequent drainback of the 1991 flow left 2–3 m of sheet flows on the floor of the trough [*Gregg et al.*, 1996]. Hydrothermal vents and biological communities imaged in 1989 [*Haymon et al.*, 1991] were covered or greatly disrupted by the new lava flows, effectively resetting the clock on the development of subsequent seafloor hydrothermal and biological systems [*Haymon et al.*, 1993].

[10] To aid in documenting the changes in the eruption area, a ~1.4 km-long transect of 210 numbered markers, the Biotransect, was deployed in early 1992 with the goal of conducting approximately annual submersible visits to record visual changes and to collect repeat hydrothermal and biological samples at specific sites [*Shank et al.*, 1998]. A number of focused flow and diffuse flow vent sites (Figure 1c) were developing when the Biotransect was deployed. Since then, some of the vents have become inactive and new ones have initiated [*Fornari et al.*, 1998, 2004]. *Von Damm and Lilley* [2004] subdivide the hydrothermal systems of the Biotransect into North, Middle, and South sections (Figure 1c), and each section has focused and diffuse flow vent sites in close proximity to one another. Hydrothermal venting in this section of the EPR is restricted to the floor or the walls of the 50–100 m wide AST, and the vents all occur close to fissures that formed the loci of eruption and lava drainback for the 1991/1992 eruptions [*Fornari et al.*, 2004]. While the immediate aftermath of the 1991 eruption brought about widespread diffuse hydrothermal outflow characterized by bacterial floc [*Haymon et al.*, 1993],

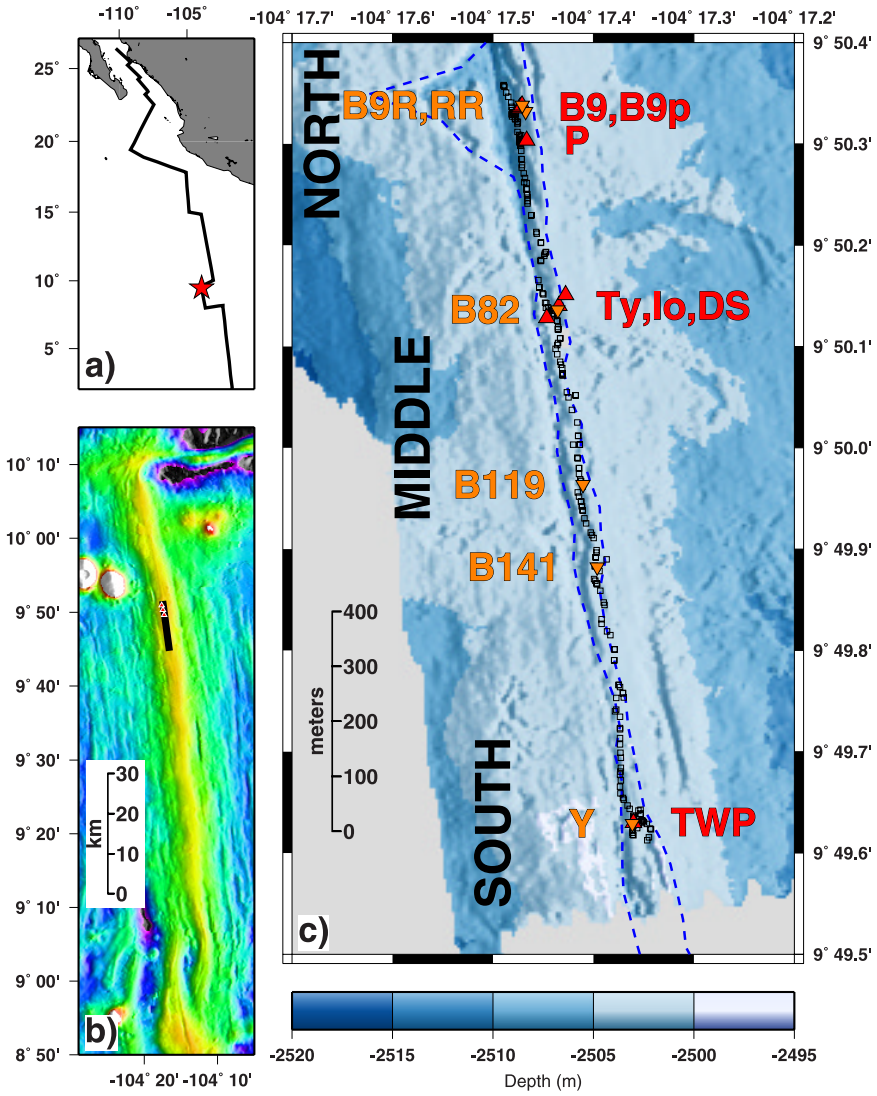

Figure 1. (a) Regional map of the East Pacific Rise north of the Equator; study site is marked by a star, just south of the Clipperton Transform Fault. (b) Bathymetry of EPR from the Clipperton Transform in the north to the 9°N OSC in the south; depth of the shallowest EPR axis is ~2500 m. Extent of 1991/1992 eruptions is shown in black, and triangles mark locations of Biovent, Bio9, and Tubeworm Pillar vent sites from north to south. (c) Map showing diffuse flow vents (orange symbols and labels) and focused flow vents (red symbols and labels). Seafloor microtopography was collected by ABE near-bottom sonar [*Schouten et al.*, 2002; *Fornari et al.*, 2004] and is artificially illuminated from the east. Dashed blue lines delineate the boundary of axial summit trough, and open squares are the Biotransect marker locations. North, Middle, and South designations of the Biotransect follow those of *Von Damm and Lilley* [2004]. Vent field abbreviations are as follows: B9R, Bio9 Riftia; RR, Rusty Riftia; B9, Bio9; B9p, Bio9prime; B82, Bio82; B119, Bio119; B141, Bio141, DS, Damoclese Sword; TWP, Tubeworm Pillar.

subsequent visits documented discrete vent fields separated by vent-free areas within the AST.

3. Measurements and Analysis

[11] In 1993, a program of monitoring the temperature of focused flow and diffuse flow fluids from vents in the 9°50′N EPR area was established using autonomous probes (Figure 2). HOBO probes were used for high-temperature vents, and Vemco Minilogger probes were used for low-temperature vents [*Fornari et al.*, 1994, 1996, 1998; *Shank et al.*, 1998]. (Any use of trade, product, or firm names is for descriptive purposes only and does not imply endorsement by the U.S. Government.) For the first three years, only a few of the vents were monitored at a coarse sample interval of ~4 hours. Since 1996, all of the vents labeled in Figure 1, along

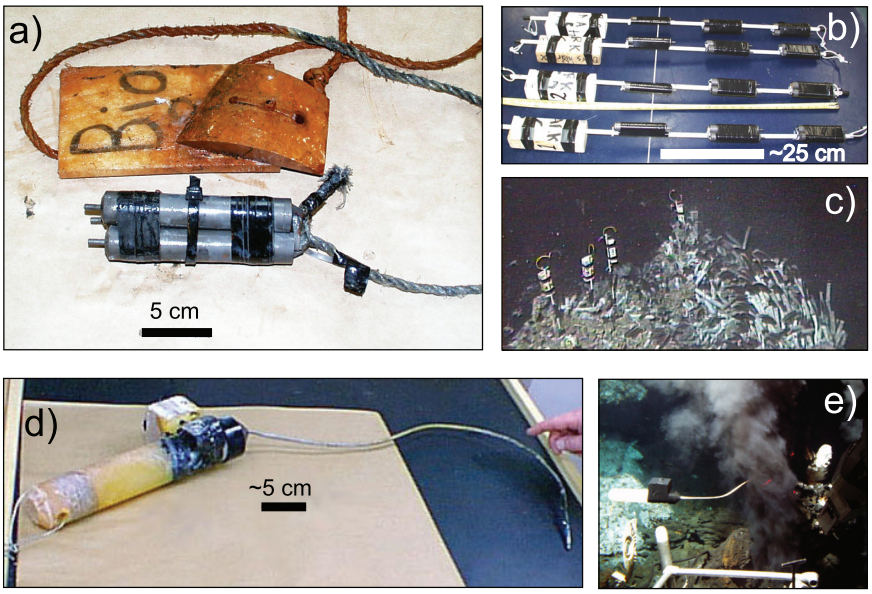

Figure 2. Photographs of low-temperature and high-temperature probes used in the EPR experiments. (a) Three low-temperature Vemco probes are bundled together and attached to a float for submersible recovery. Sensor tips extend to the left in this photo. (b) Four "stick" arrays of Vemco probes prior to their deployment at the Bio141 site in May 1999. Flotation on the left keeps the sticks upright; probe tips are toward the bottom of the sticks (right, in photo). Vemco probes measure temperatures at three levels that are separated by 23 cm; the lower two levels have two probes each. (c) *Alvin* photo of the four Vemco sticks deployed at Bio141 in May 1999. View is toward the northwest; the separation between the left stick (#1) and the right stick (#4) is about 4 m. Bottom probes of each stick are buried within the tubeworms. This photograph shows the northern half of the Bio141 community in May 1999. (d) High-temperature HOBO probe, with sensor tip at the bottom right and data logger located in the housing covered with black tape. (e) HOBO probe deployed in *P* Vent, May 1999.

with some vents to the north and the south of the Biotransect, have been monitored at sample intervals of 10–20 minutes. The durations of the temperature records range from 0.5 to 2 years, and these records are the basis for the time series analysis presented below. The probes were calibrated using ice-baths and customized ovens in the presence of calibrated thermometers. On the basis of the dynamic range of the data loggers and the expected temperature range of the monitored vents, the temperature resolution of the high-temperature probes was set to 1°C and that of the low temperature probes was set to 0.1°C. Thermal response times of the temperature probes are <1 minute based on these calibration tests. After the application of an instantaneous temperature jump to the probe tip, 50% of the temperature difference is recorded after about 8 seconds and >95% of the difference is achieved after 1 minute. Short-term probe deployments at diffuse flow vents (e.g., Figure 3a), with sample intervals between 1 and 4 seconds, indicate that aliasing of the temperature records by discrete sampling at 10–20 minutes is not a problem: namely, temperature variations at higher frequencies than can be measured by the 10–20 minute sampling are much smaller than those at lower frequencies in the measurement band (Figure 3b).

[12] Low-temperature probes (Figure 2a) were often bundled together in groups of two or three, or they were deployed as linear arrays within diffuse flow fields (Figures 2b and 2c), at positions where hydrothermal outflow was observed to be maximal. A bundle of probes allows for redundant data recording (Figures 3c and 3d) and for establishing the variability of the temperature field at small spatial scales: the sensor tips are ~2.5 cm apart within a bundle. In most cases, a single bundle was deployed in each diffuse flow vent field to capture a representative time series of the temperature fluctuations. In a few deployments, especially at the diffuse flow vent site at Biomarker 141 (Figures 1c and 2c), multiple bundles and sticks were used to define the spatial structure of the temperature field as it varied in time.

[13] High-temperature probes (Figure 2d) were deployed with the sensor tip placed in a vent orifice having vigorous flow (Figure 2e), and care was taken to redeploy in the same orifice at each vent.

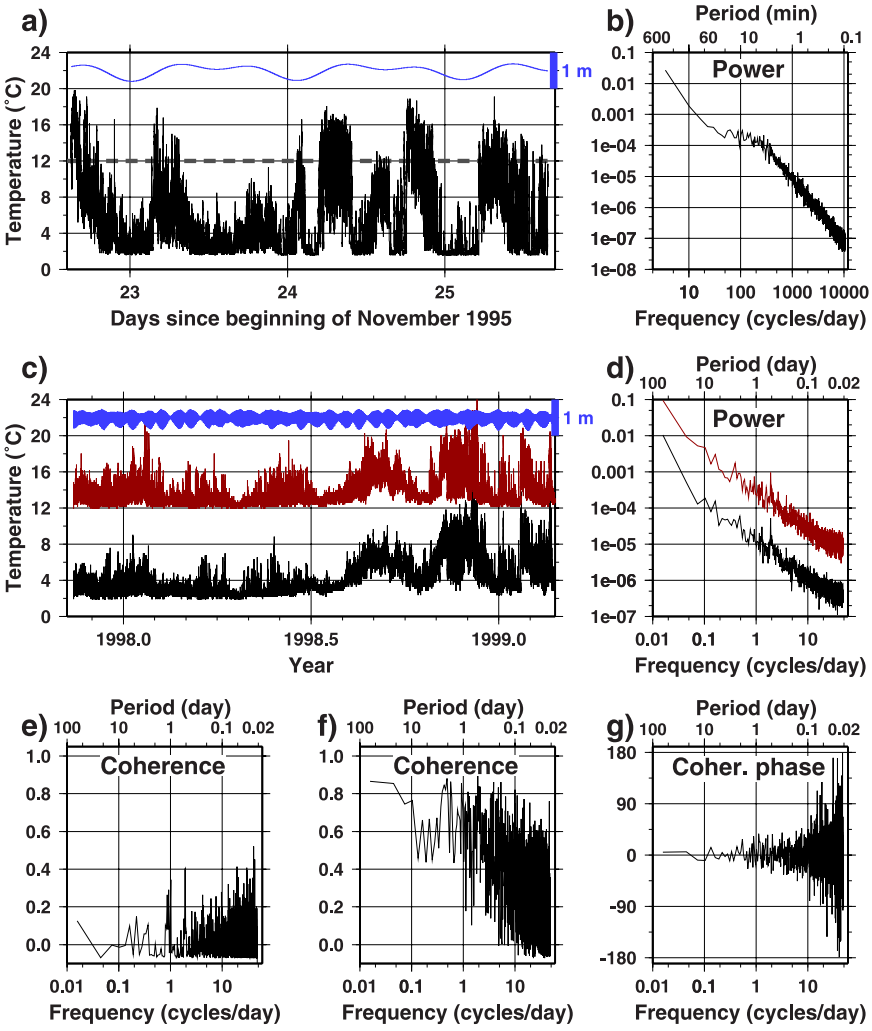

Figure 3. (a) Temperature time series of a short-term (∼3 day) and high-resolution (4-second sample interval) deployment of a Vemco probe at the Bio141 site and (b) its corresponding power spectrum. The thin, blue line in Figure 3a denotes the predicted tidal height at this site; the tidal range is 0.6 m. A ∼1.3 year time series of two, bundled Vemco probes at Bio141 is shown in Figure 3c; the red line is offset by 10°C to allow comparison of these two records from probe tips that were 2.5 cm apart. Tidal heights are displayed as in Figure 3a. Power spectra of these two temperature records are shown in Figure 3d, with the red spectrum multiplied by a factor of 200 for clarity. (e) Coherence magnitude spectrum between the temperature record (black line of Figure 3c) and the predicted tidal series. The (f) coherence magnitude and (g) phase spectra between the two temperature records displayed in Figure 3c show that they are significantly coherent and in-phase over the entire measurement band, with some degradation at frequencies >20 cycles/day (at periods <∼1 hour).

Submersible fluid sampling was done at these same orifices [*Von Damm*, 2000, 2004]. As observed during recovery operations, the probes occasionally were cemented within a growing sulfide chimney or an orifice was sealed by sulfide precipitation, leading to measurements that do not reflect variations in the hydrothermal fluid temperatures. In one deployment, a sulfide chimney toppled, ending the hydrothermal record. By inspecting temperature records collected in these cases, we identified the times when the probe stopped measuring unimpeded hydrothermal flow conditions, and we omitted those observations from further analysis.

[14] The continuous records of high-temperature and low-temperature hydrothermal data were downloaded upon probe recovery and then minimally processed to ensure that temperatures were valid for the time interval when the probe was deployed within the vent. Temperature data were then merged with a series of theoretical ocean tides [*Agnew*, 1996] (blue lines in Figures 3a and 3c)

calculated for the study site. In this mid-ocean setting, the tidal model that we used, based on satellite altimetry, generates virtually identical predicted tidal sequences to other available models.

[15] During several of the monitoring time intervals, Aandaara rotary vane current-meter data were collected at Biovent, about 1.2 km north of the Biotransect along the EPR axis [*Kim and Mullineaux*, 1998; *Marsh et al.*, 2001] (Figure 1b). These records of the horizontal near-bottom currents were corrected for magnetic deviation, interpolated across times when currents were too slow to measure with the sensor, projected into a reference frame parallel and perpendicular to the axis of spreading, and merged with the temperature and tidal series. No measurements of near-bottom currents were made at the vents of the Biotransect when their temperatures were monitored, and the geographic separation between these vents and Biovent limit the utility of comparisons of available bottom current versus vent temperature records. Thus, in this study we focus (1) on the statistical characteristics of the Biovent currents in the time and spectral domains, (2) on current meter comparisons with predicted tidal sequences, which are virtually identical between Biovent and the Biotransect vents to the south, and (3) on coherence magnitude (and not phase) relationships between Biovent currents and temperatures at one of the Biotransect vents.

[16] Time series of the temperature, predicted tides, and currents were analyzed in both the time and spectral domains. Spectral analysis was performed with conventional techniques for estimating power spectra and coherence spectra [e.g., *Bendat and Piersol*, 1980].

4. Results

4.1. Multiyear Variability of Diffuse Flow Temperatures

[17] In the decade following the 1991/1992 eruptions, the temperature evolution of diffuse flow vent fluids was complex (Figures 4 and 5). Composite temperature time series were created by manually selecting records from each vent area that have similar temperature behavior before and after redeployment. While the composite records are thus imperfect, they provide the best overview of the continuous fluid temperature behavior in different areas over time spans of many years.

[18] Discrete measurements of the maximum fluid temperatures encountered during sampling operations (red stars in Figure 4, from *Von Damm and Lilley* [2004]) exhibit a general cooling trend with time in the middle and southern portions of the Biotransect. In this sampling, diffuse flow sites were probed using a pumped manifold fluid sampler to find the highest-temperature hydrothermal outflow prior to sample collection [*Von Damm and Lilley*, 2004]. The continuous temperature records (Figure 4), with red, black, and blue lines indicating daily maximum, mean, and minimum temperatures, respectively, are more challenging to interpret because they reflect the hydrothermal flow variability in the immediate vicinity of the temperature probe tips. In some instances, we recorded temperatures in part of the vent field outside of the zone of maximum flux as measured by discrete fluid sampling (e.g., 1994–1998 in the Middle Biotransect, Figure 4b). In other cases, large and rapid temperature swings likely reflect movement of the probe tip relative to the localized hydrothermal flow pattern (e.g., Figure 4a at ~1994.5, 1996.0, 1999.5, and 2001.6). Finally, the diffuse nature of the venting prevents redeployment of probes in exactly the same positions at a given vent site. Bearing in mind these caveats and exploiting the redundant data from multiple probe deployments in the same vent field, we interpret the spatial and temporal variation of temperatures at a wide range of scales.

[19] In Figure 5, we combined individual probe records for four diffuse flow vents to show records that are as continuous as possible for each location, in terms of their minimum/mean/maximum temperature evolution. For the most part, these composite records seem to capture realistic multideployment temperature behavior, and a number of observations can be made. All of the vent fluid temperatures vary significantly over timescales of 0.5–2.0 years. While some vents have minimal (<1°C) daily temperature variation as seen in the separation between the minimum and maximum temperature curves (e.g., Bio9 Riftia during 1996.5–2001.5, Figure 5a, and Bio82 at ~1997.0, Figure 5b), others vary by much greater amounts, 5°–20°C. In some instances, diffuse fluids vary significantly in daily temperature range within a single deployment (e.g., Bio82, 1996–1997.8, Figure 5b). Many records have daily low temperatures that are pegged at the temperature of ambient seawater (1.8°C) indicating that the probe tips were not in contact with fluids having elevated temperatures for parts of many days. In other

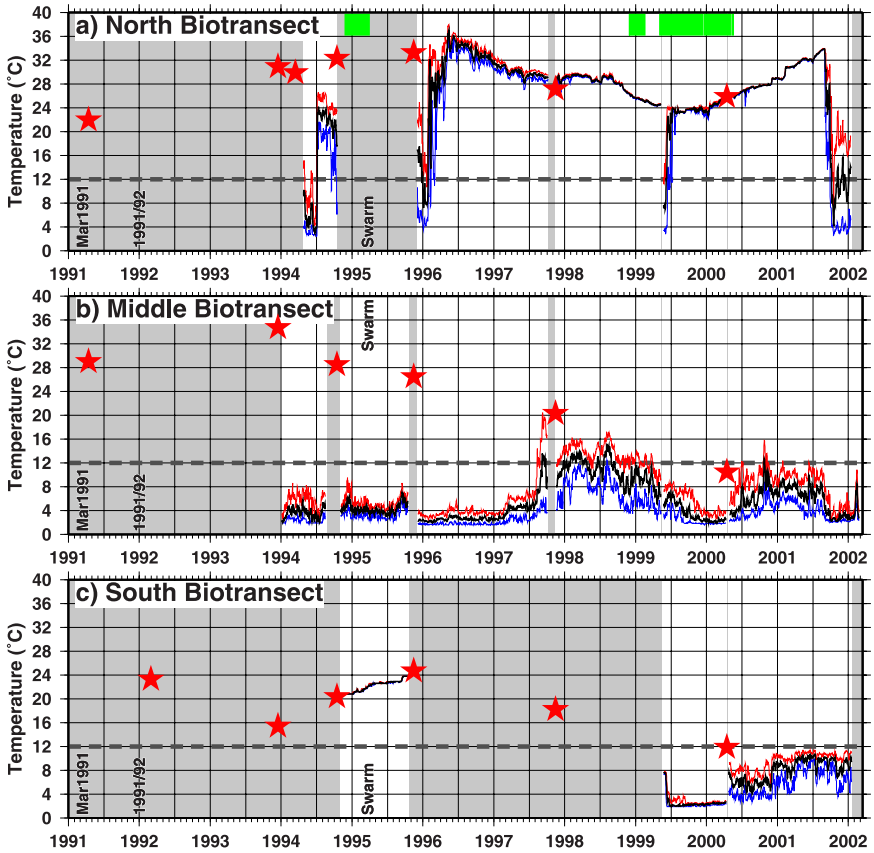

Figure 4. Temperature variation at selected diffuse flow vent sites in the (a) North, (b) Middle, and (c) South Biotransect areas of the EPR near 9°50′N prior to 2002. Black lines are the daily mean temperatures from continuous records; red lines show daily maxima, and blue lines show daily minima. The particular temperature records in this display were chosen to present as continuous a record as possible of the temperature fluctuations at each site. Temperature discontinuities exist in the records where data gaps occur (gray areas) because probes were not redeployed in exactly the same sites. Red stars are the maximum temperatures recorded by discrete measurements [*Von Damm and Lilley*, 2004]. The dashed line at 12°C represents the inferred oxic/anoxic boundary of *Johnson et al.* [1986]. The times of eruption events and the microearthquake swarm are labeled on each panel. Green bars in Figure 4a indicate time periods when near-bottom current meter data were collected at Biovent, ~1.2 km north of the Biotransect.

instances, the daily high temperatures are clipped at constant high-limit values (e.g., Bio119, 1998–2000, Figure 5c), suggesting that the probe tips were in contact only with hotter, less diluted hydrothermal fluid (i.e., not mixed with seawater after exit from the seafloor) for portions of these days. These observations are discussed below in terms of how they may reflect variable mixing ratios of ambient seawater and slowly varying low-temperature hydrothermal end-member fluids.

4.2. Subyear Variability of Diffuse Flow Temperatures

[20] The temperatures at neighboring diffuse flow vents in the Bio9 area (Figure 1) during March 2000 are illustrated in Figure 6a. The Bio9 Riftia site exhibits minimal variability, while the Rusty Riftia site ~4 m to the south exhibits an increasing daily variability, up to 8°C, toward the end of the month. The temperature difference between Rusty Riftia and ambient seawater is about half that of Bio9 Riftia and seawater. The variability of horizontal near-bottom currents at two levels above the Biovent site (~1.2 km to the north) is illustrated in Figures 6b and 6c, projected as along-axis (red) and across-axis (orange) currents. The predicted tide series (Figure 6d) is composed of diurnal and semidiurnal (twice-per-day) constituents that combine to form a tidal envelope with beating.

[21] Power spectra of selected diffuse flow temperature, current, and tide series are presented in Figure 7. The background spectra of temperature and current observations have decreasing power with increasing frequency, with a slope of

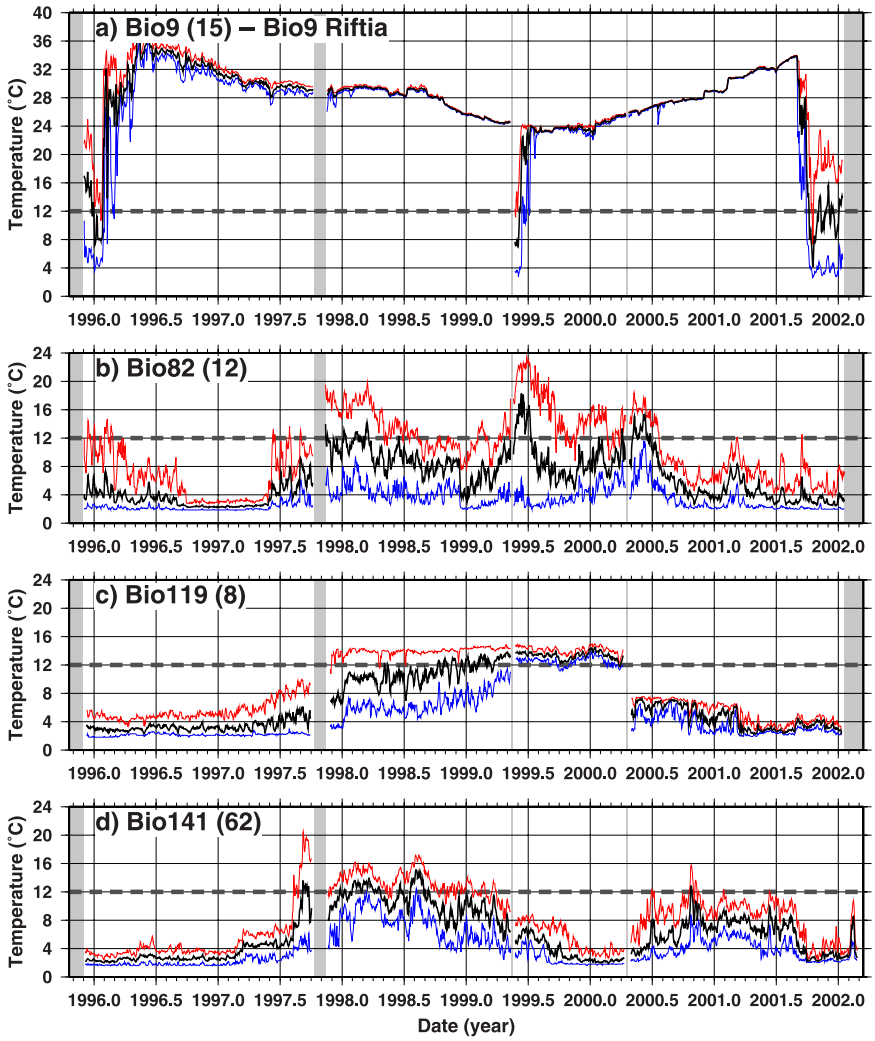

Figure 5. Temperature records from 1996 through 2001 at the four diffuse flow vent sites at the EPR near 9°50′N with the longest records. Black, red, and blue lines display daily mean, maximum, and minimum temperatures, respectively. The choice of temperature records displayed and the 12°C line are described in Figure 4.

(frequency)$^{-2}$. The spectral power of Rusty Riftia is 1–2 orders of magnitude greater than that of Bio9 Riftia at all frequencies, and Bio82 is slightly higher still. Superimposed on the background spectra of Rusty Riftia and Bio82 are small peaks at semidiurnal frequencies; the magnitude of the peaks are slightly more than half of an order of magnitude. The near-bottom current power spectra have peaks at semidiurnal, diurnal, and 0.3–0.4 cycles/day frequencies (Figures 7b and 7c); the largest are the semidiurnal peaks with sizes of about two orders of magnitude. The low-frequency peaks in the current observations are broader than the others and are centered on the Coriolis frequency at this latitude (0.34 cycles/day; 2.9 day period). Any motions excited at this near-inertial frequency will tend to persist [e.g., *Thomson et al.*, 1990]. The spectrum of the predicted tides (Figure 7d) has near-equal diurnal and semidiurnal peaks that reflect the input tidal constituents and their effects at this location.

[22] The frequency behavior of vent temperatures and near-bottom currents may be split into two spectral bands: shorter periods where variations are dominated by discrete spectral peaks at semidiurnal, diurnal, and near-inertial periods, and longer periods where variations are dominated by the higher-power and linear portions of the power spectra. For convenience, we will use the time period of a week to differentiate short-term (less than a week) from long-term (greater than a week) variability.

[23] The coherence relationships among observed temperatures, measured currents, and predicted tides also shed light on causal connections in the

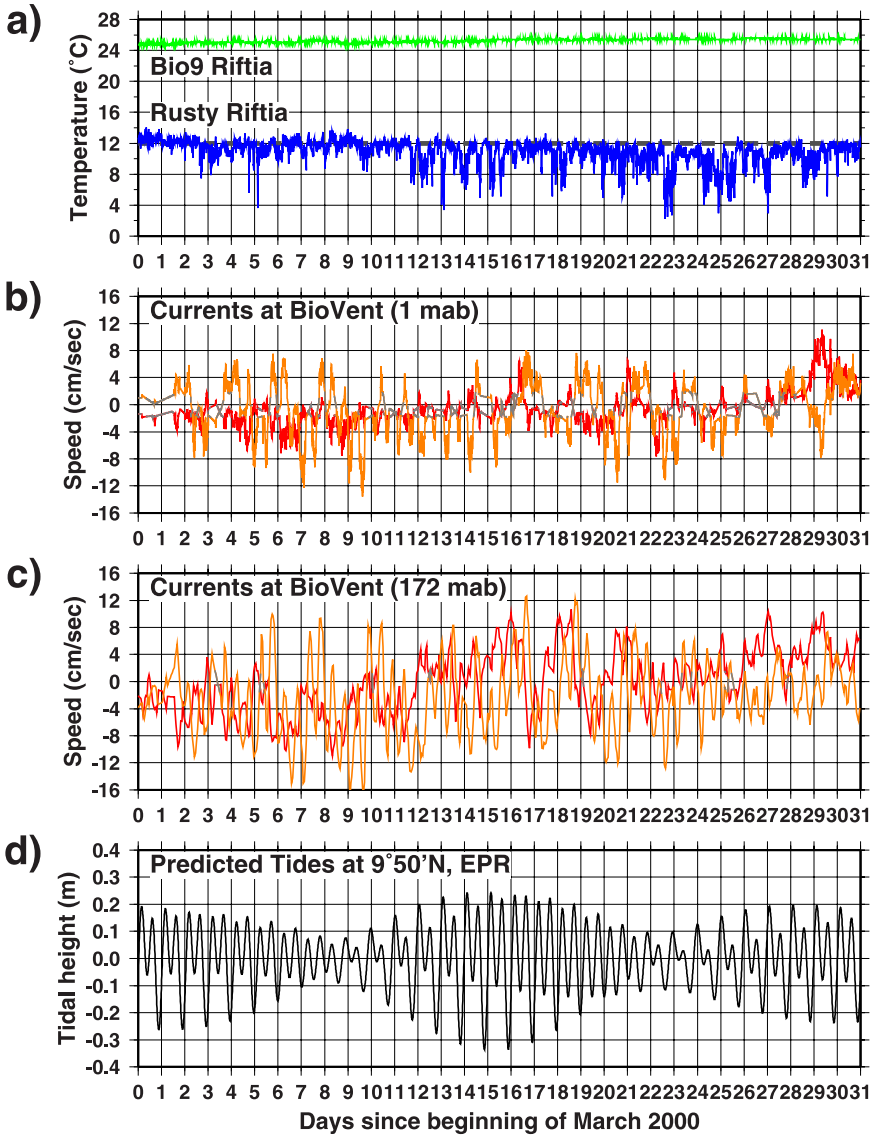

Figure 6. March 2000 time series measurements of (a) diffuse flow vent temperature at Bio9 Riftia and Rusty Riftia, (b) currents at Biovent at 1 meter above bottom (mab), (c) currents at Biovent at 172 mab, and (d) predicted tides. In the current-meter panels, the red line indicates the current speed in the along-axis direction (nearly north-south, with north-heading currents positive); the orange line indicates the current speed across-axis (nearly east-west, with east-heading currents positive). Gray lines indicate times when the magnitude of the current is below the detection threshold of the current-meter, 2 cm/s.

hydrothermal and near-bottom flow systems because they provide a statistical measure of correlations of these phenomena across the measured range of frequencies. Figures 7e and 3e illustrate that diffuse flow vent fluid temperatures at Bio82 and Bio141, respectively, have a small but non-zero coherence with the semidiurnal and diurnal predicted tides. In contrast, near-bottom horizontal currents at 1 mab and 172 mab are strongly coherent with semidiurnal and, especially, diurnal tidal fluctuations (Figures 7f and 7g). Coherence comparisons of temperatures and currents with predicted tides are meaningful only at tidal frequencies because the tidal predictions have power only at those frequencies (Figure 7d). Comparing the Bio82 temperature record with the Biovent currents at 1 mab shows low coherence throughout the spectrum (Figure 7h), although there are slight rises in coherence between temperature and both cross-axis and along-axis current at tidal frequencies. The separation of ~1.5 km between the measurements of current at Biovent and temperatures at Bio82 limit the interpretability of this coherence comparison.

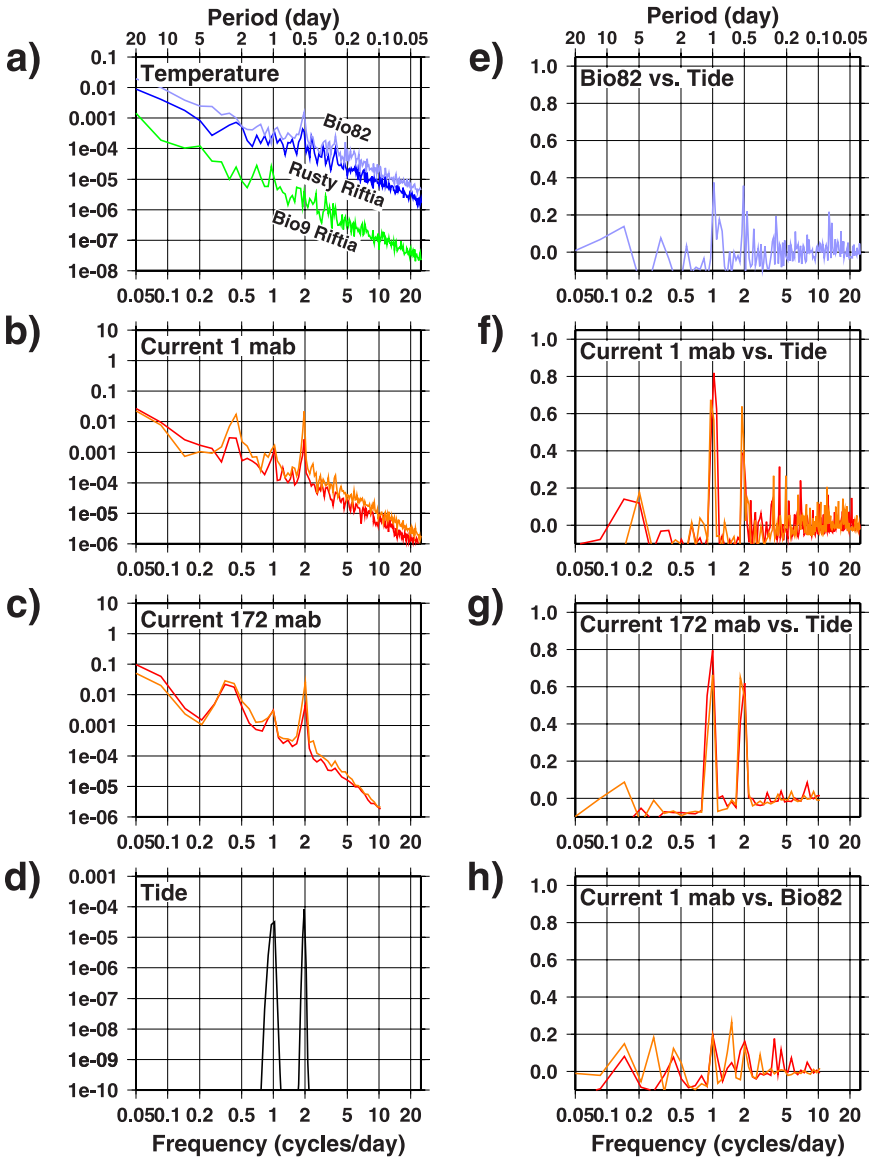

Figure 7. Power spectra of (a) diffuse flow temperature at Bio82, Rusty Riftia and Bio9 Riftia vents, (b) currents at Biovent at 1 mab, (c) currents at Biovent at 172 mab, and (d) predicted tides for the time interval from 1999/12/16 to 2000/04/15, a time span that includes the data displayed in Figure 6. Power spectral density units are $(°C)^2 \cdot d$, $(cm/s)^2 \cdot d$, and $m^2 \cdot d$, respectively. Red lines indicate currents along-axis; orange lines indicate across-axis currents. Coherence spectra of (e) diffuse flow temperature at Bio82 and predicted tide, (f) Biovent currents at 1 mab and predicted tide, (g) Biovent currents at 172 mab and predicted tide, and (h) Biovent currents at 1 mab and temperatures at Bio82 vent.

[24] Another view of the short-term temperature variability is provided by analyzing vertically-oriented arrays of probes placed in the Bio141 vent community (Figures 2c and 8). Four sticks, each with temperature probes at three levels, were placed in a line from near the center to the northern edge of the community (Figures 8a and 8b). In all cases, the lowest probes recorded the highest temperatures and the probes highest above the seafloor measured ambient seawater temperatures most of the time. While the maximum temperature decreased gradually for all of the sticks in the latter half of 1999 (Figure 8c), shorter-term fluctuations differed significantly among the sticks. For example, Stick1 and Stick2 alternately recorded the highest temperature values. Over the timescale of several days, intraday temperature variability was synchronous among the probes at different horizontal and vertical positions (Figures 8e and 8f).

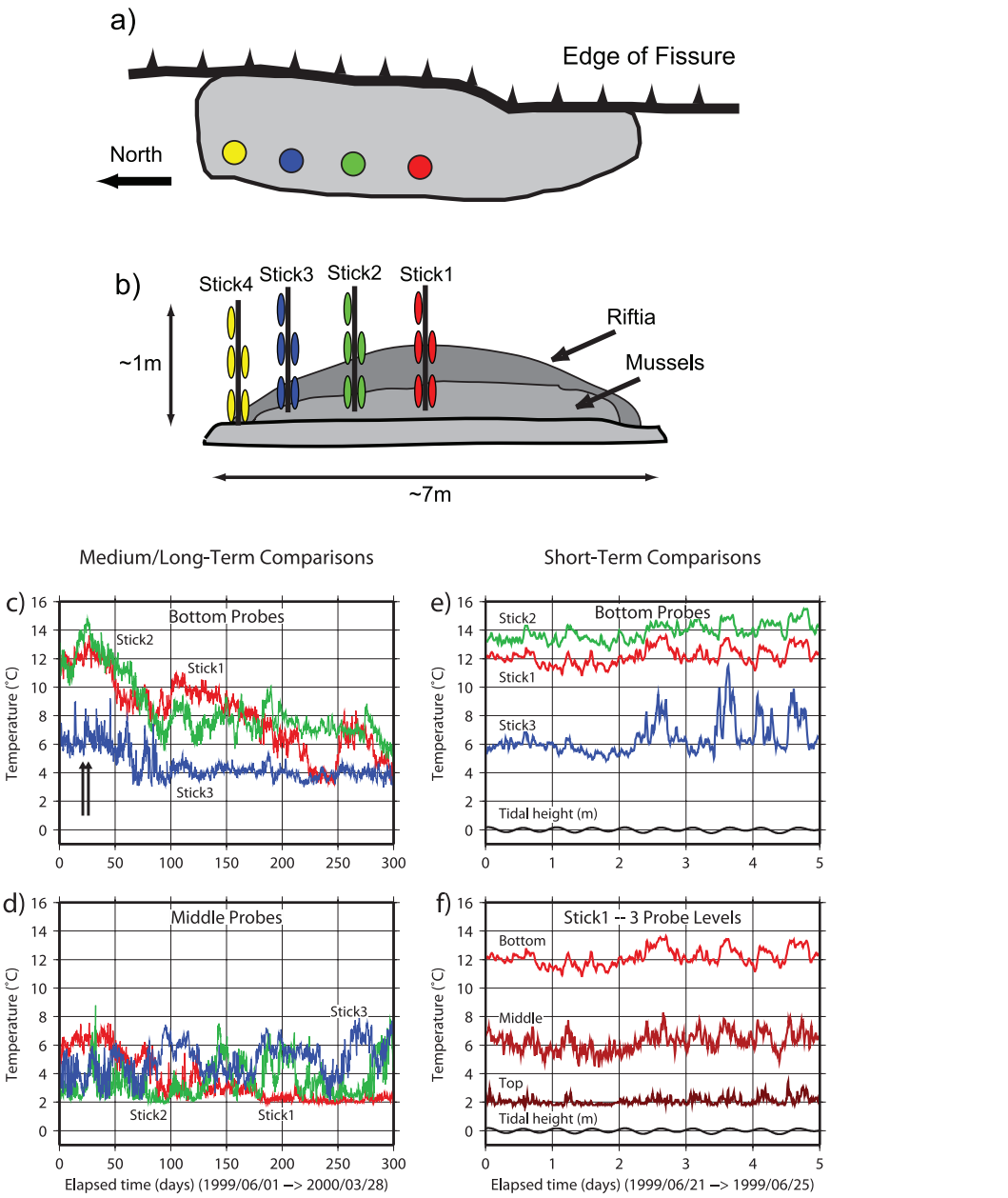

Figure 8. (a) Schematic map and (b) cross-sectional views of the Bio141 diffuse flow vent site and the positions of Vemco temperature sensors in 1999 and 2000 (see Figure 2c for *Alvin* photo of deployed probes). Elongate shapes are the temperature probes, whose sensor tips point downward. Shaded areas indicate approximate positions occupied by Riftia and mussels at the beginning of the deployment in early 1999. One year later, the volume occupied by mussels grew to encompass nearly the 1999 tubeworm volume, and the Riftia also extended upward. Vertical exaggeration is ~2x. Examples of temperature fluctuations for 300-day time spans are displayed in Figures 8c and 8d and for 5-day time spans in Figures 8e and 8f. Arrows in Figure 8c indicate the time interval displayed in Figures 8e and 8f.

4.3. Spatial Variability of Diffuse Flow Temperatures

[25] As noted above, fluid temperatures within a diffuse flow site varied systematically over vertical scales of tens of centimeters, and they were observed to vary both systematically and randomly at horizontal scales of meters. While the long-term temperature evolution was similar among probes closest to the seafloor (Figure 8c), temperatures recorded at the level of tubeworm plumes (~0.5–1.5 m above the substrate, Middle Probes) (Figure 8d) varied incoherently.

[26] At shorter distance scales, temperature records from two or more sensors deployed as a bundle

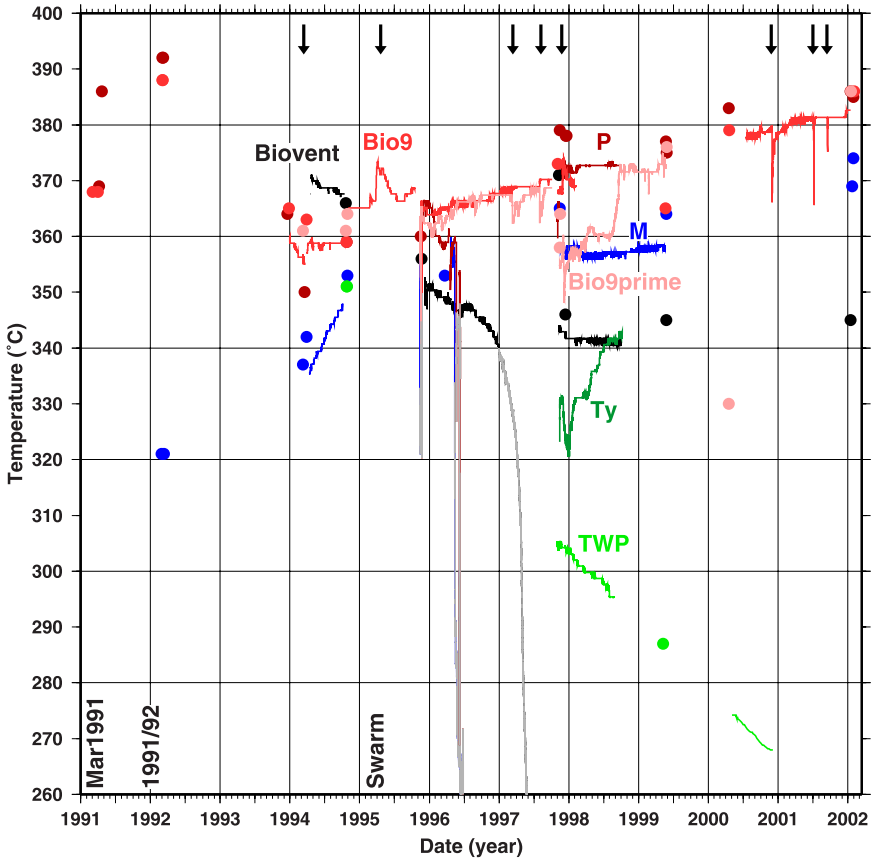

Figure 9. Fluid temperature variation between 1991 and 2002 at four focused flow, high-temperature vents in the EPR Biotransect area (Bio9, Bio9prime, P, Ty, TWP) and at two focused flow vents (Biovent, M) located ~1 km north of the northern limit of the Biotransect. Discrete measurements made while sampling fluids from these vents are shown as dots [*Von Damm*, 1995, 2000]; continuous measurements with HOBO probes are shown as colored lines. Gray lines indicate when the continuous records reflect temperatures associated with vent sealing, chimney toppling, or other causes not related to changes in the vent effluent. Arrows indicate times of temperature excursions of one or more of the vents.

(Figure 2a, probe tips are separated by 2.5 cm) were coherent and in-phase (coherence magnitude >0.5, Figures 3f and 3g). Temperatures of bundled probe tips were generally within a few tenths of a degree Celsius. In rare cases, however, temperatures of adjacent probe tips diverged by two or more degrees Celsius suggesting significant perturbations to the predominant flow conditions at those times.

[27] At diffuse flow vent sites separated by hundreds of meters, some long-term trends of warming or cooling are similar (Figure 5). In contrast, at periods of tens of days and shorter, temperature fluctuations are incoherent over those same distances (not shown).

4.4. Temporal and Spatial Variability of Focused Flow Temperatures

[28] Interpreting multiyear, composite temperature records of focused flow vents near 9°50′N on the EPR is complicated by two factors: real, short-term temperature excursions of the venting fluid and problems inherent to monitoring actively growing and collapsing sulfide structures [e.g., *Fornari et al.*, 1998]. The view of temperature evolution from discrete measurements (filled circles in Figure 9) is one of slow, multiyear evolution. In the year following the 1991/1992 eruptions, focused flow fluids at vents in the northern end of the Biotransect (Bio9 and *P* vents) were >380°C. They cooled to ~360°C after 1–2 years, then slowly warmed over the next 8 years. In contrast, the temperatures at Tubeworm Pillar decreased steadily after it was first measured in 1994. Biovent and M vent, ~1 km north of the Biotransect, show contrasting temperature evolution: Biovent cooled and M vent warmed since first observations in 1994 and 1992, respectively. Several vents, such as Ty and Io in the middle of the Biotransect, initiated in the years after the 1991 eruption. In all focused flow

areas, individual chimneys and orifices have grown and collapsed [*Fornari et al.*, 1998, 2004].

[29] Continuous monitoring of focused flow temperature yields results that are consistent with the long-term temperature evolution obtained from the discrete records (Figure 9). Significantly, continuous records also reveal more-rapid temperature fluctuations at timescales of days to months and with magnitudes of 5°–10°C, or occasionally more. In one instance, *Sohn et al.* [1998] measured a seismic swarm in the vicinity of Bio9 vent in early 1995 that preceded by 4 days a sudden, week-long 10°C rise in temperature that was followed by a slower decay to the temperature value prior to the event. The seismicity was located ~1 km below the seafloor and a few hundred meters laterally away from Bio9 vent. No diffuse flow records were collected in the Bio9 area at the time of the 1995 seismic activity nor were other focused flow vents monitored.

[30] Other short-term temperature excursions at focused flow vents occurred at Bio9 vent in early 1994, late 2000, and mid 2001 (Figure 9, arrows). These were all negative excursions, unlike the positive temperature anomaly at Bio9 in early 1995, so it is likely that they arose from a different cause, perhaps involving entrainment of cooler fluids. No other continuous high temperature records from focused flow vents (P, Bio9prime) adjacent to Bio9 vent are available to provide additional context to these excursions. In 1997, Bio9prime vent exhibited two negative temperature swings (Figure 9), neither of which was marked by unusual behavior in the Bio9 vent (<5m away) record.

4.5. Comparison of Diffuse Flow and Focused Flow Temperatures

[31] The most significant short-term temperature event recorded by multiple probes at neighboring diffuse flow and focused flow vents in the Biotransect began in November 1997 (Figures 10 and 11) when the three high-temperature vents in the northern Biotransect area (Bio9, Bio9prime, and P) all recorded temperature swings of 6–12°C over a three-week period [*Fornari et al.*, 2004]. The shapes of the temperature excursions vary considerably: Bio9prime has both positive and negative swings, Bio9 is marked by a positive excursion, and *P* vent is marked by only a few spike-like decreases (Figure 11a). For geographic reference, Bio9 and Bio9prime vents are within ~5 m of each other; *P* vent is ~50 m to the south (Figure 1). In all cases, the post-event temperature stabilized at a value very close, if not identical, to that prior to the temperature perturbation. In contrast, fluid temperatures at Biovent and M vent, over a kilometer to the north of the Biotransect, are virtually constant over this time interval. Curiously, the lower-temperature focused flow vent Ty, about 350 m south of the Bio9 vents, underwent a 2-monthlong negative temperature swing of 10°C that started at the same time as the anomalies recorded at P, Bio9 and Bio9prime (Figure 11).

[32] The temperature record from the diffuse flow Bio9 Riftia site, within ~5 m of Bio9 and Bio9-prime focused vents, exhibits a three-week temperature excursion that starts precisely with those of the adjacent focused flow vents (Figure 11b). The magnitude of the temperature swing is ~2°C, and its dipolar shape most closely resembles that of Bio9prime. Figure 11b displays records from three Vemco sensors bundled together at Bio9 Riftia, with the records successively offset by −2°C for clarity. As with most Vemco bundles, the temperatures of the different sensors agree to within a few tenths of a degree for most of the displayed time, indicating that the temperature structure of the flow does not vary significantly over the dimension of the bundle tip separations, ~2.5 cm. Among all of the EPR Vemco deployments analyzed to date, the greatest temperature differences between sensors in a single bundle were observed near the end of the 1997 temperature event (~10 December 1997), when differences of up to 4°C are observed between probes 2898 and 1112 (Figure 11b). At this time, the hydrothermal outflow dynamics of Bio9 Riftia changed, the probe placement was temporarily perturbed, or both occurred. In contrast to the marked temperature variations at Bio9 Riftia, the fluid temperatures of the diffuse flow Rusty Riftia site, within ~5 m of Bio9, Bio9prime, and Bio9 Riftia, exhibit only a small decrease in minimum and maximum temperatures coincident with those of the neighboring vents. The temperature fluctuation at Rusty Riftia of 1°–2°C is the same as the vent's daily fluctuations of (Figure 11c), so the temperature excursion is not obvious by examining the Rusty Riftia record alone.

5. Discussion

5.1. Origin of Long-Term Temperature Variability at Diffuse Flow Vents

[33] Temperatures at individual locations in EPR diffuse vent fields vary by small amounts over time

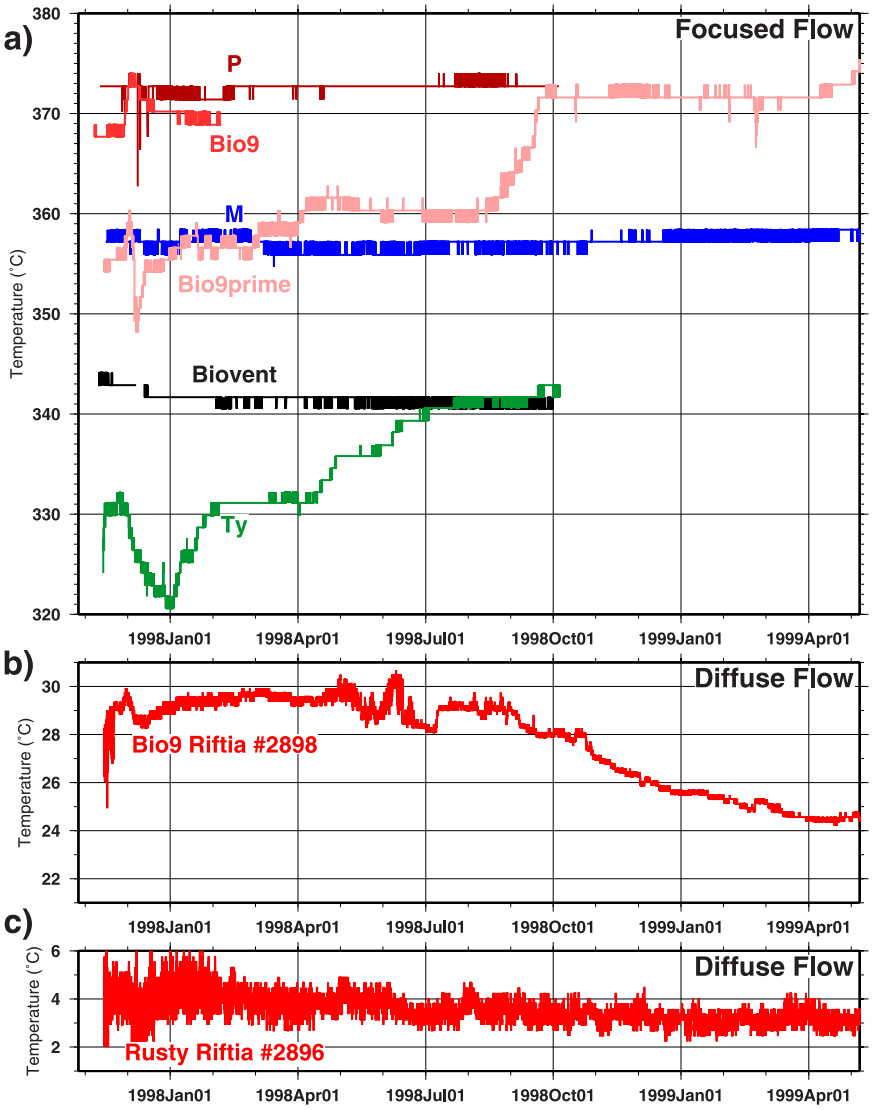

Figure 10. (a) High-temperature HOBO probe data for the time interval between October 1997 and June 1998 show the temperature excursions recorded by Bio9, Bio9prime, Ty, and, to a lesser extent, *P* vents, while the more distant Biovent and M vent recorded near-constant temperatures at the 1°C precision. (b) Vemco temperature probe data for the Bio9 Riftia diffuse flow vent community that is adjacent to the Bio9 and Bio9prime high-temperature vents. (c) Vemco temperature probe data for the Rusty Riftia diffuse flow vent community that is also adjacent to the Bio9 and Bio9prime high-temperature vents. Temperature records from some vents are terminated because of battery or memory failures within the logger during the deployment.

periods of weeks to years, whereas they vary greatly at periods less than a few days. The controls on temperatures within diffuse flow fields at long periods are likely to be related to the primary heat source at depth, the nature of subsurface fluid pathways and reservoirs, and the modification of these physical conditions by volcanic, tectonic, and depositional processes. After the 1991/1992 EPR eruptions, the highest temperatures in the three main diffuse flow regions of the Biotransect decreased in the ensuing decade (Figure 4, stars). This likely reflects either a slow decrease in the temperature of the heat source that drives hydrothermal circulation, a cooling of crustal host-rock, a gradual increase in dilution of hydrothermal fluids with ambient seawater in the uppermost oceanic crust prior to venting, or a combination of these factors.

[34] Over time spans of weeks and months, individual vent areas exhibit distinct cooling behavior, and multiple vents within a single site may have disparate fluid temperature histories (Figures 4 and 5). This observation is consistent with geochemical

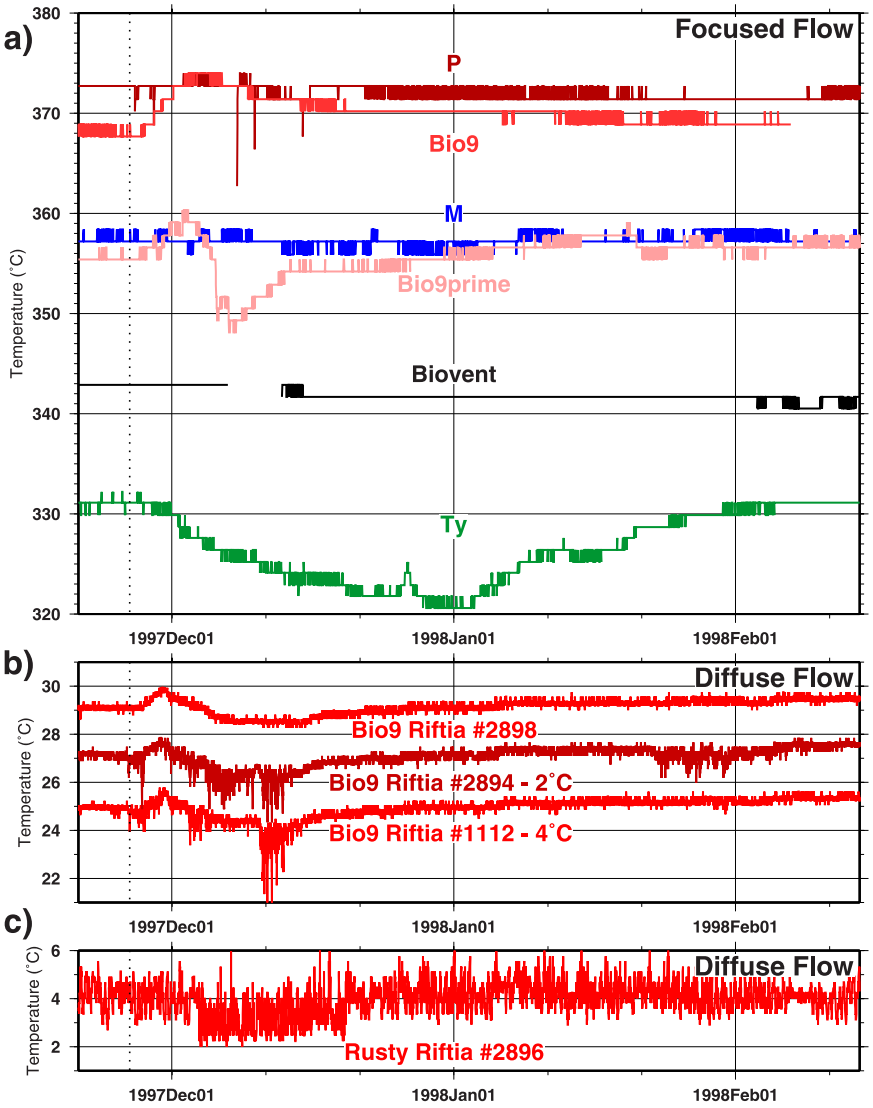

Figure 11. Same data as in Figure 10, expanding the time between November 1997 and February 1998. In Figure 11b, all three Vemco records from a bundle are displayed, with the lower two successively offset by −2°C for clarity. Dotted vertical line indicates the start of 1997 November 27.

variation and trends in evolutionary behavior of the fluids sampled at these diffuse vents [*Von Damm and Lilley*, 2004]. In addition, *Von Damm and Lilley* [2004] observe that concentrations of CH_4, H_2S, and H_2 of diffuse fluids differ from expected values if their formation were governed by simple, conservative mixing between high-temperature fluids, akin to those venting at focused vents, and ambient seawater. They interpret these departures as evidence for subsurface biological activity, which in turn suggests the importance of fluid residence in a reservoir beneath the seafloor for some time prior to venting. While temperature monitoring alone cannot determine the presence of such a reservoir, measuring the delay times and spatial patterns of diffuse flow temperature response following an independently determined event (e.g., seismically detected volcanic, intrusive, or tectonic activity) provides strong constraints on the hydrologic properties of any subseafloor reservoir [e.g., *Wilcock*, 2004].

5.2. Oxic and Anoxic Environments Near Diffuse Flow Vents

[35] *Johnson et al.* [1986, 1988] sampled fluids at the Rose Garden diffuse flow site on the Galápagos Spreading Center and determined that hydrothermal fluids with temperatures >12°C were anoxic, whereas those <12°C contained significant dissolved oxygen. The 12°C threshold is highlighted

on all of the time series plots to indicate a potential boundary between oxic and anoxic waters. While this threshold may not be exactly 12°C at 9°50′N EPR, adjusting this temperature by 1–2°C would not change our interpretations of the biological significance of diffuse fluid temperatures. Many of the 9°50′N EPR vents recorded times when, within the span of a day, a probe sampled temperatures both close to ambient seawater and at or above the inferred 12°C anoxic threshold. This condition indicates optimal habitat for vent megafauna that are reliant on chemosynthetic symbionts. This observation is consistent both with the placement of the temperature probes among tubeworm and mussel aggregations and with the recruitment of many individuals on the probe housings during the 0.5–2 year durations of deployment (T. M. Shank et al., Influences of temperature and chemistry on habitat selection at hydrothermal vents, manuscript in preparation, 2006; hereinafter referred to as Shank et al., manuscript in preparation, 2006).

[36] The Bio9 Riftia diffuse flow vent was the only site with extended periods when temperatures were restricted to the higher, anoxic realm. After mid-1996, all measured temperatures were >24°C and daily temperature variability is minimal (Figures 4 and 5), except for a few, limited periods when there was a rapid change to significantly lower and more variable temperature conditions. During a November 1995 *Alvin* dive prior to Bio9 Riftia's elevated temperature phase, a thriving *Riftia pachyptila* community was observed. The community structure represented a culmination of a four-year sequence of development at this location that started with no megafauna immediately after the volcanic eruption, followed by colonization of *Tevnia jerichonana*, then replacement by *Riftia*, and finally expansion of the colonized area of *Riftia* [*Shank et al.*, 1998]. In November 1997 on the first *Alvin* dive to the Bio9 Riftia site following the early-1996 temperature increase, a die-off of a significant fraction of the tubeworms had occurred. By May 1999, the Bio9 Riftia site was devoid of life due to vent effluent that was constantly anoxic and iron rich [*Von Damm and Lilley*, 2004; Shank et al., manuscript in preparation, 2006].

5.3. Origin of Short-Term Variability at Diffuse Flow Vents

[37] At timescales of less than a week, diffuse fluid temperatures vary significantly and systematically within a vent field. Most of this variability is coherent with near-bottom currents at periods excited by the tides (diurnal and semidiurnal) and at periods centered on the Coriolis frequency (~3 days at 9°–10°N).

[38] To explain a 12-day temperature record of a Guaymas Basin diffuse flow vent, *Little et al.* [1991] proposed the conceptual model of a thermal boundary layer that is created by vent effluent injected into ambient bottom water and is distorted laterally with near-bottom tidal currents. We extend this model to include non-tidal bottom currents, especially those at near-inertial periods, and to allow the temperature of primary vent effluent to vary on timescales of weeks and longer (Figure 12a). By including these dynamic effects, our model explains many of the observations from the time series fluid temperature data collected at the 9°50′N EPR diffuse flow hydrothermal sites. A complete characterization of this thermal boundary layer model would require monitoring of temperatures throughout and surrounding individual vent fields, as well as measurement of near-bottom currents adjacent to each site.

[39] Monitoring of the Bio141 site by multiple probes on four vertically-oriented sticks (Figure 2c and Figure 8) provides insight into the nature of the thermal boundary layer formed by hydrothermal upflow from the seafloor into near-bottom waters. At Bio141, the lens of elevated temperatures extends only ~0.5 m above the base of the sticks (Figure 8f), which were placed as close to the sites of seafloor venting as possible. Thus the vertical dimension of the lens is 0.5–1.0 m above the seafloor. The distribution of megafauna delimits the dimensions and position of the thermal boundary layer (Figures 2c and 8). The warmest hydrothermal temperatures occur at sites closest to the center of the biological community (Figures 8c and 8e), but through time the site of highest measured temperature varies laterally by meters. At Bio141 during the stick deployments, beds of mussels constituted the base of the faunal aggregation, and tubeworms extended to higher levels. Other vent endemic and related organisms were observed in niches associated with these dominant fauna. The changing position of the biomass, especially the mussel aggregations, influences the permeability structure and consequent temperatures measured by the probes. This behavior likely explains the similar temperature behaviors of the bottom probes at Bio141 (Figure 8c) versus the different temperature behaviors of the middle probes (Figure 8d) that are situated

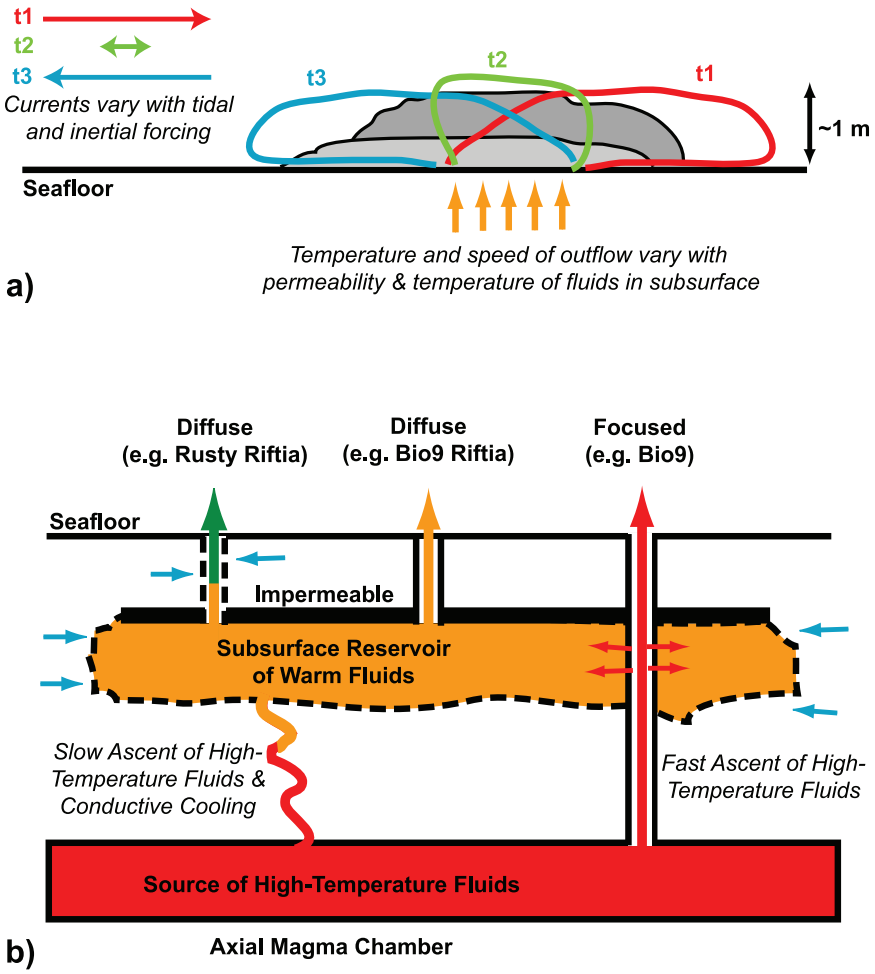

Figure 12. (a) Conceptual model of the thermal boundary layer at a diffuse flow vent site for three different near-bottom current patterns at different time instants: t1, t2, t3. Gray fields delineate megafauna occurrence, e.g., a lower zone of mussels and a higher zone of tubeworms. Colored outlines represent the periphery of waters having hydrothermal fluid components; hydrothermal fluids increase in concentration toward the seafloor site of venting (orange arrows). (b) Schematic model of subsurface fluid discharge pathways above a magma chamber, highlighting a shallow reservoir and its various inputs of hydrothermal fluids from depth and from leaky focused flow conduits and of seawater that fills adjacent porosity. In this cartoon, dashed lines indicate permeable boundaries, red arrows indicate high-temperature fluid motion, blue arrows indicate flow of cold ambient seawater in the subsurface, and the depth, orientation, and lateral extent of the reservoir boundaries are unknown.

above the mussels and among the tubeworm plumes.

[40] Synchronous temperature fluctuations on different sticks at Bio141 over timescales of days indicate that near-bottom currents advect warmer hydrothermal fluids from the center of the vent site toward its periphery (Figures 8e and 13a). The limited rise of elevated temperatures (Figure 8f) indicates that the upward flow rate of hydrothermal fluids that are passing through the faunal community is smaller than the typical horizontal speed of near-bottom currents, 5–10 cm/s (Figure 6b). This is opposite the behavior at focused flow vents where upward advection is sufficient to produce vertical rise of many tens to hundreds of meters and where plume rise is terminated by mixing and neutral buoyancy rather than horizontal advection and distension of the hydrothermal volume [e.g., *Baker et al.*, 1993].

5.4. Geologic Indicators of Subsurface Permeability Structure

[41] A major control on the initiation and evolution of seafloor hydrothermal systems is the permeability structure of young oceanic crust, which is created by volcanic and tectonic processes at the

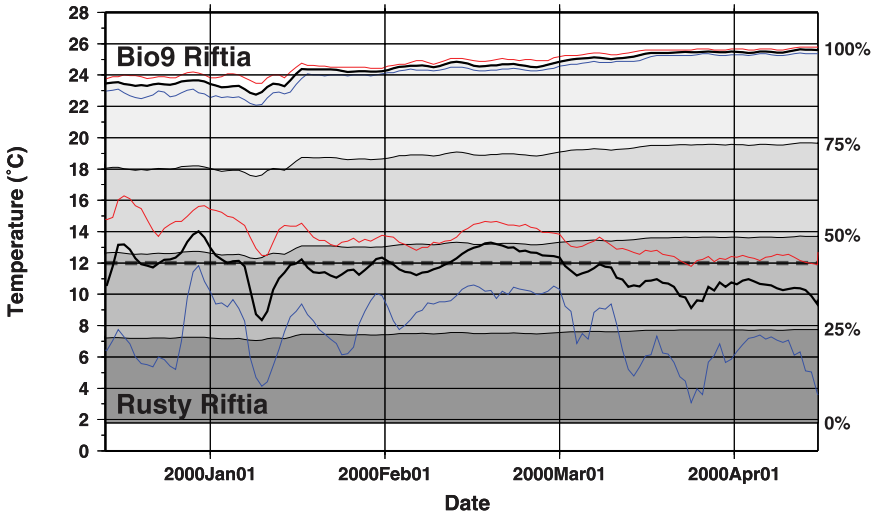

Figure 13. Temperature variation at the adjacent Bio9 Riftia and Rusty Riftia diffuse flow sites, displayed as daily mean, max, and min values (black, red, blue lines) for a ~4 month period in late 1999 and early 2000. Gray fields indicate mixing proportions, between 0% and 100%, of undiluted hydrothermal fluid (as represented by the Bio9 Riftia vent) and seawater (at 1.8°C), if temperature is a conservative mixing property in this setting.

axis and modified by hydrothermal deposition and off-axis constructional and mass-wasting processes [*Carbotte and Scheirer*, 2004]. At 9°50′N EPR, heterogeneous and anisotropic permeability structure is primarily derived from volcanic stratigraphy (largely horizontal) and from fissuring (largely vertical). Individual eruptions inflate, collapse, and form networks of lava tubes and/or surface flows, both within the AST and away from the axis [e.g., *Fornari et al.*, 2004]. Subsequent eruptions fill some of the former void-space. Dikes and eruptive fissures provide the pathways for magmas to rise from the axial magma chamber at >1 km depth, and they also accommodate post-eruptive drainback [*Haymon et al.*, 1993; *Gregg et al.*, 1996]. The fissures furnish vertical permeability directly above the magmatic heat source, although magma solidification within the fissure disrupts this permeability. Tectonic fissures [*Wright*, 1998] also provide vertical permeability, although they are generally not as deep as their eruptive counterparts and they occur at locations where magmatic activity is currently low. In the Biotransect, all of the diffuse and focused flow hydrothermal vents occur within the AST along the 1991/1992 eruptive fissure. This demonstrates the importance of vertical permeability directly above the magmatic heat source in governing the distribution of hydrothermal venting at the seafloor. That said, the localization of hydrothermal outflow at discrete sites above the magmatic heat source indicates that impermeable layers must be present in the upper oceanic crust and that vertical pathways have limited lateral extent. Away from the 1991/1992 eruptions, other EPR vents are associated with fissures within or along the walls of the AST.

5.5. Insights Into Subsurface Permeability Provided by Adjacent Diffuse Flow Vents

[42] The Bio9 Riftia and Rusty Riftia diffuse flow vent sites are situated within 4 m of each other along the 1991/1992 eruptive fissure. In the first half of 1996, Bio9 Riftia vent fluid temperatures increased and their daily range decreased, which was followed by five years of slow variations in fluid temperatures greater than 20°C (Figure 5). Over the same time interval, Rusty Riftia fluid temperatures fluctuated consistently between about 4° and 14°C (not shown). To explain these differences, we appeal to the existence of a shallow subsurface hydrothermal fluid reservoir, as inferred from vent fluid geochemistry in this area [*Von Damm and Lilley*, 2004; *Shank et al.*, 1998], which is tapped differently by Bio9 Riftia and Rusty Riftia (Figure 12b). A similar configuration is suggested for Yellowstone hydrothermal systems [*Fournier*, 1989]. We infer that the pathways feeding Rusty Riftia from the subsurface reservoir of warm fluids entrain a significant fraction of ambient seawater that fills voids in the uppermost crust. In contrast, the pathways feeding Bio9 Riftia have much less horizontal permeability, which allows venting of fluids more representative of those in the subsurface reservoir.

[43] From late December 1999 to mid-April 2000, the subsurface reservoir temperature appears to have increased by about 2°C (Figure 13, Bio9 Riftia record). This interpreted increase falls within a longer time interval when the neighboring Bio9 and Bio9prime focused flow vents were also slowly increasing in temperature (Figure 9), although continuous records of the high-temperature vents are not available in late 1999 and early 2000. Alternatively, the subsurface reservoir temperature may have been constant, while the degree of armoring of the conduit leading to Bio9 Riftia may have increased, thereby reducing dilution with cooler fluids in the uppermost crust. Regardless of the particular explanation of the Bio9 Riftia temperature rise, the coincident decrease in temperature of Rusty Riftia (Figure 13) suggests that this vent became progressively more diluted by ambient seawater. Assuming that temperature behaves conservatively and that Bio9 Riftia fluids are an accurate proxy of the reservoir fluid, then the proportion of warm hydrothermal fluid at Rusty Riftia decreased from an average of about 50% to an average of 30% from late 1999 through the first part of 2000 (Figure 13, Rusty Riftia black line). If the maximum Rusty Riftia temperature (Figure 13, red line) is a more appropriate measure of the mixing fraction, then the proportion of hydrothermal fluid decreased from ~60% to ~40%. Given the rise in temperature at Bio9 Riftia, the progressive cooling at Rusty Riftia likely involved an increase in the flux of ambient seawater into the hydrothermal upflow conduit (Figure 12b).

[44] The existence and importance of a permeable zone in the uppermost oceanic crust that serves as a reservoir of hydrothermal fluids and as a region of physical, chemical, and biological reaction is emerging in many studies of both near-spreading ridge and old crust [e.g., *Mottl and Wheat*, 1994; *Cowen et al.*, 2003; *Johnson and Pruis*, 2003]. In near-axis regions, this concept is motivating theoretical studies of the poroelastic response of oceanic crust and hydrothermal systems to pressure fluctuations due to tides [*Jupp and Schultz*, 2004; *Crone and Wilcock*, 2005]. In these models, the vertical and horizontal variations in permeability are critical parameters to determine whether or not tidal pumping is an important modulator of hydrothermal flux. *Pruis and Johnson* [2004] examined diffuse flow from seafloor cracks on Axial Seamount, Juan de Fuca Ridge, by affixing a hydrologically sealed instrument to the seafloor and directly measuring effluent temperature and velocity. This type of sampler effectively separates the subseafloor temperature variations of fluid exiting the seafloor from the effects of variable mixing with ambient seawater in changing near-bottom currents, overcoming a limitation of the temperature-only studies such as the present one, *Little et al.* [1991], and *Tivey et al.* [2002]. On Axial Seamount, a small proportion of the temperature variations of diffuse flow fluids can be attributed to poroelastic tidal response [*Pruis and Johnson*, 2004].

5.6. Insights Into Subsurface Permeability Provided by Adjacent Diffuse and Focused Flow Vents

[45] The coincident onset of temperature excursions (Figure 11) at the focused flow Bio9, Bio9-prime, and *P* vents and at the diffuse flow Bio9 Riftia vent demonstrates that the plumbing systems feeding these vents are at times interconnected. The three-week long temperature perturbation that started on 27 November 1997 was detected on the vents in the northern Biotransect, even though the shape and the magnitude of the temperature fluctuations varied among the vents. In the subsurface model proposed above, high-temperature fluids that exit the seafloor at focused flow vents are thought to originate from levels close to the magmatic heat source and to flow upward within conduits where there is minimal cooling and exchange with adjacent pore fluids (Figure 12b). The late 1997 temperature event likely represents an ephemeral perturbation of the permeability structure feeding the diffuse flow and focused flow vents because the temperature swings are both positive and negative and because the vents return to pre-event temperatures within a few weeks, a short time period relative to the cooling time of all but the smallest igneous intrusions at depth.

[46] The negative temperature excursion at Ty vent, ~500 m south of the vents in the northern Biotransect, starts within a day or two of the other temperature events, but it extends for a longer time period of about two months (Figure 11). With the existing temperature data, it is difficult to explain the connections, if any, between the Ty temperature anomaly and the similar-magnitude but shorter anomalies at Bio9 and Bio9prime. The Bio82 diffuse flow vent adjacent to Ty does not show a temperature excursion during this time (Figure 5b), unlike the synchronous anomalies seen in the northern Biotransect diffuse flow vents (Figure 11). This observation suggests that the cause of the Ty anomaly may be distant from Ty. Because temperature

excursions were absent at Tubeworm Pillar (~900 m south of Ty and ~1400 m south of Bio9) and at M and Biovent (~800 m and ~1000 m north of Bio9, respectively), the source of the anomaly may be centered close to Bio9 with an along-axis influence of at least 500 m and at most about 800 m. This placement and influence of the anomaly source is inconsistent, however, with the observation that *P* vent, which is only ~50 m south of the Bio9 and Bio9prime vents, exhibits a temperature anomaly that is much-diminished in magnitude and duration (Figure 11). This, in turn, suggests that the lateral influence of the source of the Bio9-area temperature excursions is on the scale of tens, rather than hundreds, of meters and that the Ty event is unrelated. These divergent interpretations demonstrate that while continuous temperature data can detect and provide glimpses into the processes that perturb hydrothermal systems, more observations of other aspects of the system are required for improved understanding.

[47] The best example of insights from complementary data at 9°50′N EPR is provided by the early 1995 seismic swarm, which allowed *Sohn et al.* [1998] and *Fornari et al.* [1998] to interpret a downward-propagating crustal cracking event that tapped into hot rock and raised the temperatures of effluent before returning to the prior temperatures in the next 2–3 months. This event also perturbed the stable isotopic composition of vent fluids [*Shanks*, 2001]. *Wilcock* [2004] successfully modeled the properties of this high-temperature transient: its delayed onset after the seismic swarm, its magnitude, and its decay, using a temperature perturbation model whereby a new crack connects a fluid reaction zone at depth to the focused flow vent at the surface.

6. Conclusions

[48] Continuous monitoring of diffuse and focused flow hydrothermal vent fields in the years following a MOR volcanic eruption provides insights into the subsurface processes and structures that govern the formation and evolution of hydrothermal vents and their associated biological communities. At diffuse flow vents, horizontal advection of hydrothermal fluids by near-bottom currents is important for providing an environment where sessile and sedentary vent endemic fauna can exploit alternating periods of both anoxic (for chemosynthetic symbiont sustenance) and oxic (for metabolism) conditions that are necessary for life. The presence of a shallow subsurface reservoir of warm hydrothermal fluids can explain the disparate but related temperature fluctuations observed in neighboring diffuse flow and focused flow vent fluids. This reservoir may be created by the ascent and cooling of deeper, higher-temperature fluids and by mixing with cooler waters within large-scale voids created by intraflow and inter-flow permeability in the shallow ocean crust at fast spreading MORs [e.g., *Fornari et al.*, 2004]. The position, dimensions, and ubiquity of a subsurface reservoir are unknown, but its existence is also suggested by geochemical and microbial evidence in hydrothermal fluids.

[49] The logistical challenges of continuous monitoring of focused and diffuse flow vents arise from the dynamic environment created by the interactions of vertical and horizontal currents, by the growth and collapse of hydrothermal precipitate structures, and by the development of faunal communities. Notwithstanding these difficulties, continuous temperature records provide a new perspective on the timescales and interactions of a rich array of igneous, tectonic, oceanographic, and biological processes. In the future, time series vent fluid temperature monitoring will benefit from complementary data sets for fluid chemistry (e.g., pH, chlorinity, H_2S), microseismicity, near-bottom oceanographic conditions, and photographic documentation of faunal community development.

Acknowledgments

[50] We are grateful for the cruise opportunities and dive time provided by many colleagues to conduct the temperature probe operations. The skill and patience of the pilots in the *Alvin* at-sea operations group, under Expedition Leader Pat Hickey, in deploying and recovering the probes was instrumental to the success of our studies. We thank the shipboard and shore-based crews of R/V *Atlantis* and *Alvin* for their dedication and expertise that resulted in collection of the data reported here. We are grateful to Mark Olsson and his colleagues at DeepSea Power & Light for their collaboration in developing the temperature probes, and we thank Lauren Mullineaux for providing the EPR current-meter records. Field and shore-based analyses have been supported by the National Science Foundation (OCE-0096468, OCE-8917311, OCE-9217026, OCE-9302205, OCE-0327261), the Woods Hole Oceanographic Institution's Vetlesen Fund and W. A. Clark Senior Scientist Chair (DJF), and the Devonshire Foundation (TMS). We are grateful for reviews by Randy Koski, Pat Shanks, and two anonymous reviewers.

References

Agnew, D. C. (1996), SPOTL: Some programs for ocean-tide loading, *SIO Ref. Ser.*, *96-8*, 35 pp., Scripps Inst. of Oceanogr., La Jolla, Calif.

Baker, E. T., G. J. Massoth, S. L. Walker, and R. W. Embley (1993), A method for quantitatively estimating diffuse and discrete discharge, *Earth Planet. Sci. Lett.*, *118*, 235–249.

Bendat, J. S., and A. G. Piersol (1980), *Engineering Applications of Correlation and Spectral Analysis*, 302 pp, John Wiley, Hoboken, N. J.

Carbotte, S. M., and D. S. Scheirer (2004), Variability of ocean crustal structure created along the global mid-ocean ridge, in *Hydrology of the Oceanic Lithosphere*, edited by E. E. Davis and H. Elderfield, pp. 59–107, Cambridge Univ. Press, New York.

Copley, J. T. P., P. A. Tyler, C. L. Van Dover, A. Schultz, P. Dickson, S. Singh, and M. Sulanowska (1999), Sub-annual temporal variation in faunal distributions at the TAG hydrothermal mound (26°N, Mid-Atlantic Ridge), *Mar. Ecol.*, *20*, 291–306.

Corliss, J. B., et al. (1979), Submarine thermal springs on the Galápagos Rift, *Science*, *203*, 1073–1083.

Cowen, J. P., S. J. Giovannoni, F. Kenig, H. P. Johnson, D. Butterfield, M. S. Rappe, M. Hutnat, and P. Lam (2003), Fluids from aging ocean crust that support microbial life, *Science*, *299*, 120–123.

Crone, T. J., and W. S. D. Wilcock (2005), Modeling the effects of tidal loading on mid-ocean ridge hydrothermal systems, *Geochem. Geophys. Geosyst.*, *6*, Q07001, doi:10.1029/2004GC000905.

Dziak, R. P., C. G. Fox, and R. W. Embley (1999), The January 1998 earthquake swarm at Axial Volcano, Juan de Fuca Ridge: Hydroacoustic evidence of seafloor volcanic activity, *Geophys. Res. Lett.*, *26*, 3429–3432.

Dziak, R. P., W. W. Chadwick Jr., C. G. Fox, and R. W. Embley (2003), Hydrothermal temperature changes at the southern Juan de Fuca Ridge associated with Mw 6.2 Blanco Transform earthquake, *Geology*, *31*, 119–122.

Fornari, D. J., C. L. Van Dover, T. Shank, R. Lutz, and M. Olsson (1994), A versatile, low-cost temperature sensing device for time-series measurements at deep sea hydrothermal vents, *BRIDGE Newsl.*, *6*, 37–40.

Fornari, D. J., F. Voegeli, and M. Olsson (1996), Improved low-cost, time-lapse temperature loggers for deep ocean and sea floor observatory monitoring, *RIDGE Events*, *7*, 13–16.

Fornari, D. J., T. Shank, K. L. Von Damm, T. K. P. Gregg, M. Lilley, G. Levai, A. Bray, R. M. Haymon, M. R. Perfit, and R. Lutz (1998), Time-series temperature measurements at high-temperature hydrothermal vents, East Pacific Rise 9°49′–51′N: Monitoring a crustal cracking event, *Earth Planet. Sci. Lett.*, *160*, 419–431.

Fornari, D. J., et al. (2004), Submarine lava flow emplacement at the East Pacific Rise 9°50′N: Implications for uppermost ocean crust stratigraphy and hydrothermal fluid circulation, in *Mid-Ocean Ridges: Hydrothermal Interactions Between the Lithosphere and Oceans*, *Geophys. Monogr. Ser.*, vol. 148, edited by C. German et al., pp. 187–217, AGU, Washington, D. C.

Fournier, R. O. (1989), Geochemistry and dynamics of the Yellowstone National Park hydrothermal system, Wyoming, *Annu. Rev. Earth Planet. Sci.*, *17*, 13–53.

Fox, C. G., H. Matsumoto, and T.-K. A. Lau (2001), Monitoring Pacific Ocean seismicity from an autonomous hydrophone array, *J. Geophys. Res*, *106*, 4183–4206.

Fujioka, K., K. Kobayashi, and A. Nishizawa (1997), Tide-related variability of TAG hydrothermal activity observed by deep-sea monitoring system and OBSH, *Earth Planet. Sci. Lett.*, *153*, 239–244.

Gregg, T. K. P., D. J. Fornari, M. R. Perfit, R. M. Haymon, and J. H. Fink (1996), Rapid emplacement of a mid-ocean ridge lava flow on the East Pacific Rise at 9°46′–51′N, *Earth Planet. Sci. Lett.*, *144*, E1–E7.

Haymon, R. M., D. J. Fornari, M. H. Edwards, S. Carbotte, D. Wright, and K. C. Macdonald (1991), Hydrothermal vent distribution along the East Pacific Rise crest (9°09′–54′N) and its relationship to magmatic and tectonic processes on fast-spreading mid-ocean ridges, *Earth Planet. Sci. Lett.*, *104*, 513–534.

Haymon, R. M., et al. (1993), Volcanic eruption of the mid-ocean ridge along the East Pacific Rise crest at 9°45–52′N: Direct submersible observations of seafloor phenomena associated with an eruption event in April, 1991, *Earth Planet. Sci. Lett.*, *119*, 85–101.

Johnson, H. P., and M. J. Pruis (2003), Fluxes of fluid and heat from the oceanic crustal reservoir, *Earth Planet. Sci. Lett.*, *216*, 565–574.

Johnson, H. P., M. Hutnak, C. G. Fox, I. Urchuyo, J. P. Cowen, J. Nabelek, and C. Fisher (2000), Earthquake-induced changes in a hydrothermal system on the Juan de Fuca mid-ocean ridge, *Nature*, *407*, 174–177.

Johnson, K. S., C. L. Beehler, C. M. Sakamoto-Arnold, and J. J. Childress (1986), In situ measurements of chemical distributions in a deep-sea hydrothermal vent, *Science*, *231*, 1139–1141.

Johnson, K. S., J. J. Childress, and C. L. Beehler (1988), Short-term temperature variability in the Rose Garden hydrothermal vent field: An unstable deep-sea environment, *Deep Sea Res., Part A*, *35*, 1711–1721.

Jupp, T. E., and A. Schultz (2004), A poroelastic model for the tidal modulation of seafloor hydrothermal systems, *J. Geophys. Res.*, *109*, B03105, doi:10.1029/2003JB002583.

Kim, S., and L. S. Mullineaux (1998), Distribution and near-bottom transport of larvae and other plankton at hydrothermal vents, *Deep Sea Res., Part II*, *45*, 423–440.

Langseth, M. G., and R. P. von Herzen (1970), Heat flow through the floor of the world oceans, in *The Sea*, edited by A. E. Maxwell, pp. 299–352, Wiley Interscience, Hoboken, N. J.

Little, S. A., K. D. Stolzenbach, and F. J. Grassle (1991), Tidal current effect on temperature in diffuse hydrothermal flow: Guaymas Basin, *Geophys. Res. Lett.*, *15*, 1491–1494.

Luther, G. W., III, T. F. Rozan, M. Taillefert, D. B. Nuzzio, C. Di Meo, T. M. Shank, R. A. Lutz, and S. C. Cary (2001), Chemical speciation drives hydrothermal vent ecology, *Nature*, *410*, 813–816.

Lutz, R. A., T. M. Shank, D. J. Fornari, R. M. Haymon, M. D. Lilley, K. V. Von Damm, and D. Desbruyeres (1994), Rapid growth at deep-sea vents, *Nature*, *371*, 663–664.

Marsh, A. G., L. S. Mullineaux, C. M. Young, and D. T. Manahan (2001), Larval dispersal potential of the tubeworm *Riftia pachyptila* at deep-sea hydrothermal vents, *Nature*, *411*, 77–80.

Mottl, M. J., and C. G. Wheat (1994), Hydrothermal circulation through mid-ocean ridge flanks: Fluxes of heat and magnesium, *Geochim. Cosmochim. Acta*, *58*, 2225–2237.

Mullineaux, L. S., S. W. Mills, and E. Goldman (1998), Recruitment variation during a pilot colonization study of hydrothermal vents (9°50′N, East Pacific Rise), *Deep Sea Res., Part II*, *45*, 441–464.

Pruis, M. J., and H. P. Johnson (2004), Tapping into the subseafloor: Examining diffuse flow and temperature from an active seamount on the Juan de Fuca Ridge, *Earth Planet. Sci. Lett*, *217*, 379–388.

Reves-Sohn, R., S. Humphris, and J. P. Canales (2005), Stochastic analysis of exit-fluid temperature and time-series data from the TAG hydrothermal mound: Events, states, and hid-

den Markov models, *Eos Trans. AGU*, *86*(18), Jt. Assem. Suppl., Abstract OS22A-06.

Rubin, K. H., J. D. Macdougall, and M. R. Perfit (1994), ^{210}Po-^{210}Pb dating of recent volcanic eruptions on the sea floor, *Nature*, *368*, 841–844.

Sarrazin, J., and S. K. Juniper (1999), Biological characteristics of a hydrothermal edifice mosaic community, *Mar. Ecol. Prog. Ser.*, *185*, 1–19.

Schouten, H., M. Tivey, D. Fornari, D. Yoerger, A. Bradley, P. Johnson, M. Edwards, and T. Kurokawa (2002), Lava transport and accumulation processes on EPR 9°27′N to 10°N: Interpretations based on recent near-bottom sonar imaging and seafloor observations using ABE, Alvin, and a new Digital Deep Sea Camera, *Eos Trans. AGU*, *83*(47), Fall Meet. Suppl., Abstract T11C-1262.

Schultz, A., J. R. Delaney, and R. E. McDuff (1992), On the partitioning of heat flux between diffuse and point source seafloor venting, *J. Geophys. Res.*, *97*, 12,299–12,314.

Schultz, A., P. Dickson, and H. Elderfield (1996), Temporal variations in diffuse hydrothermal flow at TAG, *Geophys. Res. Lett.*, *23*, 3471–3474.

Shank, T. M., D. J. Fornari, and R. A. Lutz (1997), Periodicities and variability of high and low-temperature hydrothermal venting along the Biotransect (9°50′N) on the East Pacific Rise: Three years of continuous synchronous temperature monitoring, *Eos Trans. AGU*, *78*(46), Fall Meet. Suppl., F739.

Shank, T. M., D. J. Fornari, K. L. Von Damm, M. D. Lilley, R. M. Haymon, and R. A. Lutz (1998), Temporal and spatial patterns of biological community development at nascent deep-sea hydrothermal vents along the East Pacific Rise, *Deep Sea Res., Part II*, *45*, 465–515.

Shanks, W. C., III (2001), Stable isotopes in seafloor hydrothermal systems: Vent fluids, hydrothermal deposits, hydrothermal alteration, and microbial processes, in *Stable Isotope Geochemistry*, edited by J. W. Valley and D. R. Cole, *Rev. Mineral. Geochem.*, *43*, 469–526.

Shanks, W. C., III, J. K. Bohlke, and R. R. Seal II (1995), Stable isotopes in mid-ocean ridge hydrothermal systems: Interactions between fluids, minerals, and organisms, in *Physical, Chemical, Biological, and Geological Interactions Within Seafloor Hydrothermal Systems*, *Geophys. Mon. Ser.*, vol. 91, edited by S. E. Humphris et al., pp. 194–221, AGU, Washington, D. C.

Smith, D. K., M. Tolstoy, C. G. Fox, D. R. Bohnenstiehl, H. Matsumoto, and M. J. Fowler (2002), Hydroacoustic monitoring of seismicity at the slow-spreading Mid-Atlantic Ridge, *Geophys. Res. Lett.*, *29*(11), 1518, doi:10.1029/2001GL013912.

Sohn, R., D. J. Fornari, K. Von Damm, S. Webb, and J. Hildebrand (1998), Seismic and hydrothermal evidence for a propagating cracking event on the East Pacific Rise crest at 9°50′N, *Nature*, *396*, 159–161.

Thomson, R. E., S. E. Roth, and J. Dymond (1990), Near-inertial motions over a mid-ocean ridge: Effects of topography and hydrothermal plumes, *J. Geophys. Res.*, *95*, 7261–7278.

Tivey, M. K., A. M. Bradley, T. M. Joyce, and D. Kadko (2002), Insights into tide-related variability at seafloor hydrothermal vents from time-series temperature measurements, *Earth Planet. Sci. Lett.*, *202*, 693–707.

Von Damm, K. L. (1995), Controls on the chemistry and temporal variability of seafloor hydrothermal fluids, in *Physical, Chemical, Biological, and Geological Interactions Within Seafloor Hydrothermal Systems*, *Geophys. Mon. Ser.*, vol. 91, edited by S. E. Humphris et al., pp. 222–247, AGU, Washington, D. C.

Von Damm, K. L. (2000), Chemistry of hydrothermal fluids from 9–10°N, East Pacific Rise: "Time Zero" the immediate post-eruptive period, *J. Geophys. Res.*, *105*, 11,203–11,222.

Von Damm, K. L. (2004), Evolution of the hydrothermal system at East Pacific Rise 9°50′N: Geochemical evidence for changes in the upper oceanic crust, in *Mid-Ocean Ridges: Hydrothermal Interactions Between the Lithosphere and Oceans*, *Geophys. Mon. Ser.*, vol. 148, edited by C. German et al., pp. 285–304, AGU, Washington, D. C.

Von Damm, K. L., and M. D. Lilley (2004), Diffuse flow hydrothermal fluids from 9°50′N East Pacific Rise: Origin, evolution, and biogeochemical controls, in *The Subsurface Biosphere at Mid-Ocean Ridges*, *Geophys. Mon. Ser.*, vol. 144, edited by W. S. D. Wilcock et al., pp. 243–266, AGU, Washington, D. C.

Wilcock, W. S. D. (2004), Physical response of mid-ocean ridge hydrothermal systems to local earthquakes, *Geochem. Geophys. Geosyst.*, *5*, Q11009, doi:10.1029/2004GC000701.

Wright, D. J. (1998), Formation and development of fissures at the East Pacific Rise: Implications for faulting and magmatism at mid-ocean ridges, in *Faulting and Magmatism at Mid-Ocean Ridges*, *Geophys. Mon. Ser.*, vol. 106, edited by W. R. Buck et al., pp. 137–151, AGU, Washington, D. C.